Miner Deposita (2017) 52:1–34
DOI 10.1007/s00126-016-0650-3

ARTICLE

The high-grade Las Cruces copper deposit, Spain: a product of secondary enrichment in an evolving basin

Fernando Tornos[1] · Francisco Velasco[2] · John F. Slack[3] · Antonio Delgado[4] · Nieves Gomez-Miguelez[5] · Juan Manuel Escobar[6] · Carmelo Gomez[6]

Received: 18 November 2015 / Accepted: 14 March 2016 / Published online: 19 April 2016
© Springer-Verlag Berlin Heidelberg 2016

Abstract The Las Cruces deposit (Iberian Pyrite Belt) includes a large, high-grade cementation zone capped by unusual rocks that contain carbonates, galena, iron sulphides, and quartz. Between the Late Cretaceous(?) and Tortonian, the volcanogenic massive sulphides were exhumed and affected by subaerial oxidation that formed paired cementation and gossan zones. Onset of Alpine extension produced accelerated growth of the cementation zone along extensional faults, leading to formation of the high-grade copper ore at ca. 11 Ma. Later, replacement of the overlying gossan by sulphide- and carbonate-rich rocks beneath sealing marl sediments is thought to have involved microbial processes, occurring between the Messinian (ca. 7.2 Ma) and today. Isotope data show that the cementation zone formed by the mixing of descending acidic waters derived from oxidation of the massive sulphides, with upwelling geothermal waters flowing at temperatures above 100 °C. The C, O, and Sr isotope values of the mineralization ($^{87}Sr/^{86}Sr$ 0.7101–0.7104) and of the local groundwater (0.7102–0.7104) reflect equilibration with basement rocks, and indicate that influence on the ore-forming process by marl-equilibrated water (0.7091–0.7093) or Miocene seawater (0.7086–0.7092) was negligible. The high sulphur isotope values of the sulphides in the biogenic zone (most +19 to +24‰) are well above those of the primary sulphides ($\delta^{34}S$ ca. −6.8 to +10.3‰) and likely reflect formation of the biogenic sulphides by reduction of aqueous sulphate in the groundwaters. Sulphur isotope values of the cementation zone ($\delta^{34}S$ ca. −2.4 to +21.7‰) are also consistent with some contribution of sulphur from the biogenic reduction of aqueous sulphate.

Editorial handling: A. Gilg

Electronic supplementary material The online version of this article (doi:10.1007/s00126-016-0650-3) contains supplementary material, which is available to authorized users.

✉ Fernando Tornos
f.tornos@csic.es

[1] Centro de Astrobiología (CSIC-INTA), Ctra Ajalvir km. 4.5, Torrejon de Ardoz 28850 Madrid, Spain

[2] Dpto. de Mineralogía y Petrología, Facultad de Ciencia y Tecnología, Universidad del País Vasco UPV/EHU, 48080 Bilbao, Spain

[3] U.S. Geological Survey, National Center, MS 954, Reston, VA 20192, USA

[4] Laboratorio de Biogeoquímica de Isótopos Estables, Instituto Andaluz de Ciencias de la Tierra (CSIC-UGR), Avda. de las Palmeras, 4, 18100, Armilla Granada, Spain

[5] C\ Diecinueve de Octubre, 13, 24008 León, Spain

[6] Cobre Las Cruces S.A., Gerena 41860 Seville, Spain

Introduction

The Las Cruces copper deposit is located in the southeastern part of the Iberian Pyrite Belt (IPB), 20 km north-northwest of Seville (Fig. 1). This deposit, exploited by the most recent mining operation in the area, has an estimated original resource of 16 Mt of ore at an average grade of 6.9 % Cu in the secondary enrichment zone, and is one of the richest large copper deposits worldwide. This resource includes ca. 2.35 Mt of high-grade ore having more than 10 % Cu and located in the center of the orebody and ca. 0.8 Mt at 8 % Cu in a separate covellite-rich orebody called HC4. In addition, the Las Cruces deposit has ca. 1.83 Mt of "gossan" mineralization averaging 1.88 % Pb, 0.2 % Cu, 2.32 g/t Au, and 40 g/t Ag. Underlying primary massive sulphides contain an estimated resource of 38 Mt at 1.02 % Cu, 2.7 % Zn, 1.3 % Pb, 30 g/t Ag, and 0.3 g/t Au (www.first-quantum.com). The

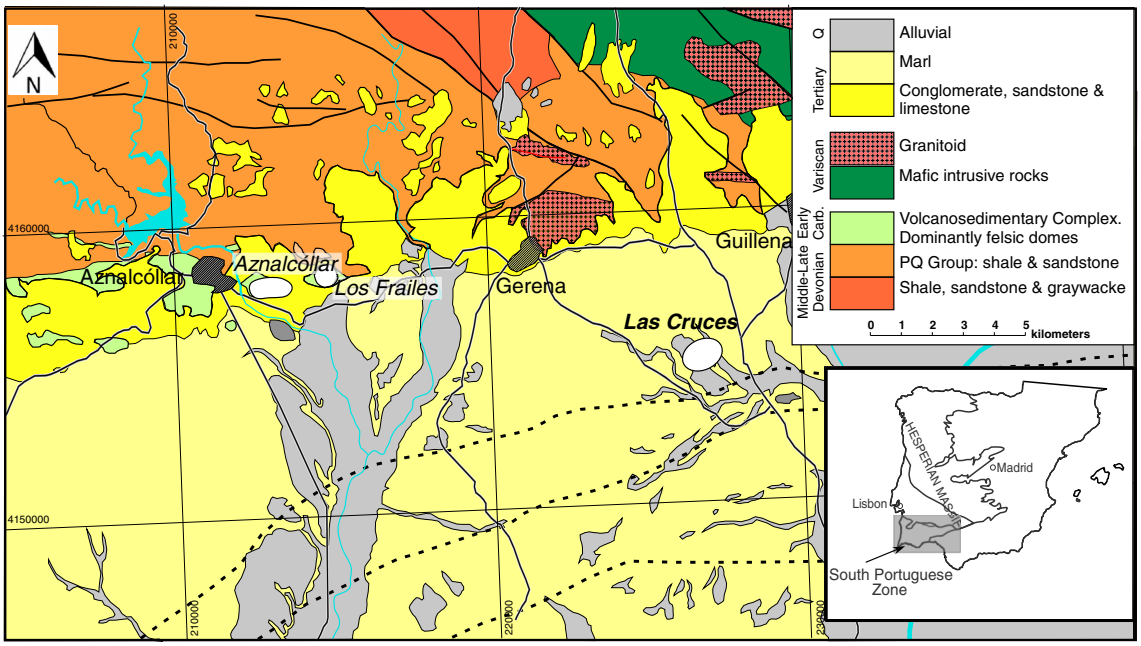

Fig. 1 Geological map of study area showing the location of major massive sulphide orebodies of the SE Iberian Pyrite Belt (based on IGME 2010). *Inset* shows the location of the Iberian Pyrite Belt on the Iberian Peninsula. *Dotted lines* are the inferred Alpine faults below the Tertiary sedimentary cover

deposit was discovered in September of 1994 by Riomin Exploraciones SA (a subsidiary of Rio Tinto), during the drilling of a large gravity anomaly below Cenozoic sediments of the Guadalquivir Basin. Since June of 2009, the deposit has been mined in an open pit by Cobre Las Cruces SA, currently a subsidiary of First Quantum Minerals Ltd. Considering only the secondary ore, the mine has a projected life until 2022. The mine will produce ca. 1 Mt of copper cathodes from the hydrometallurgical recovery of leachable copper.

One of the striking features of the Las Cruces deposit is the presence of very different types of mineralization (Table 1). The primary late Paleozoic volcanogenic massive sulphides occur within a folded and thrusted sequence of dacite and shale underlain by an irregular but large zone of sulphide-bearing stockwork. However, what makes Las Cruces unusual is a capping subhorizontal secondary zone that includes a lower cementation zone superimposed by a complex zone of red and black rocks rich in lead and precious metals, collectively included in the gossan (Figs. 2, 3, and 4). It has not been until recently, when the orebody was exposed due to mining, that a complete view is possible of the relationships between the different types of mineralization and the host rocks.

Since its discovery and first description by Doyle (1996), the Las Cruces deposit has been the focus of several remarkable studies that have proposed very different genetic models, including Knight (2000), Blake (2008), Tornos et al. (2013), and Yesares et al. (2015). Knight (2000) made a general study of the deposit based on samples from drill core, proposing seven different stages of mineralization and suggesting that the unusual secondary mineralization was in part formed during the submarine oxidation that took place in the sulphide mound soon after deposition of the primary massive sulphides; this model includes later modification of the secondary mineralization during subaerial exposure and late burial. Blake (2008) made a detailed mineralogical study and identified most of the phases present in the deposit. He suggested that the mineralogy and geochemical profile of the gossan were the result of near-surface weathering related to biogenic activity. Other studies have dealt with the geology of the orebody (Knight et al. 1999; Tornos et al. 2012a, b, 2013; Yesares et al. 2015), geologic setting of the primary mineralization (Conde et al. 2003, 2007), the gossan (Capitán et al. 2004; Yesares et al. 2011a; Tornos et al. 2014), or the mining project (Doyle 1996; Doyle et al. 2003). The recent work of Yesares et al. (2014) describes the mineralogy of the gold in the secondary zone, and with the accompanying work of Yesares et al. (2015) proposes that the formation of the secondary deposit is related to the circulation of downward flowing surficial waters that cut the Tertiary sediments. Other studies have dealt with Cu isotopes (Miguélez et al. 2012a, b), the influence of biologic activity (Tornos et al. 2011, 2014), and the timing of mineralization (Moreno et al. 2003). Significantly, genetic models vary greatly among the different authors.

In this study, we present an evolutionary model based on detailed field work and geochemistry of the deposit. Our conclusion is that Las Cruces is unique because it is the product of the maturation of a Variscan massive sulphide orebody directly related to the evolution of the hosting Tertiary foreland

Table 1 Simplified types of mineralization at Las Cruces

	Mineralization	Metal assemblage	Genesis	Fluids	Age	*T* °C	Comments
I	Volcanogenic massive sulphides	Cu–Zn–Pb–(Au–Ag)	Sub-exhalative massive sulphides formed in an (anoxic) seafloor located in the contact between a rhyodacite dome and shale	Deep hydrothermal fluids mixing with modified seawater	Late Devonian	60–250 °C[a]	No evidences of seafloor oxidation
II	Gossan/ Cementation Zone	Pb–Ba (As–Sb–Hg–Ag–Au)/Cu–(As–Sb)	Subaerial exposition and weathering of the massive sulphides. Formation of typical supergene profile in a tropical? weather	Acid descending groundwater and reaction with massive sulphides below the water table	Miocene?	Surface temperature	Local remnants of the old classical cementation zone. This event dominates in other deposits of the IPB and takes place till today
III	Advanced Cementation Zone	Cu–(As–Sb)	Accelerated formation of a cementation zone related to extensional faulting with drop of water table	Mixing of acid descending groundwater with deep hot and alkaline silica-saturated metal-rich basinal fluids (Deep Reservoir?)	10.8 ± 0.1 to 11.2 ± 0.2 Ma	Up to > 100 °C	Underlain by advanced argillic alteration. Formation of a large subaerial gossan that was later eroded
IV	Epithermal veins		Fluid mixing along fractures during waning stages of major faulting	Mixing of alkaline descending groundwater (equivalent to the Niebla-Posadas aquifer with deep hot and alkaline silica-saturated metal-rich basinal fluids) (Deep Reservoir?)	Messinian (7.2–5.3 Ma)?		Postdates burial and gossan formation. Includes both quartz-barite-calcite veins and later botryoidal growth of sulphides in open spaces
V	Biogenic Zone	Pb–Ba (As–Sb–Hg–Ag–Au)	Replacement of the gossan during microbial reduction by a sulphide-carbonate assemblage below the marl	Alkaline groundwater (Niebla Posadas aquifer)	Messinian-Actual	20–30 °C	Minor late oxidation

[a] Based on similar deposits of the southern Iberian Pyrite Belt. Tornos (2006)

basin, which influenced hydrogeology, biogenic activity, and secondary ore-forming processes in the deposit.

Geological setting

The IPB forms part of the South Portuguese Zone, the southernmost terrane of the Variscan Belt of Europe (Oliveira 1990; Fig. 1). The IPB probably was a microplate with Avalonian affinities that collided with the autochthonous Iberian Terrane in Variscan times. Synchronous with the oblique collision during the late Devonian-early Carboniferous, several continental pull-apart basins were formed. These basins were the loci of widespread, basaltic to rhyolitic volcanism and hydrothermal activity. More details on the geology of the IPB can be found in Barriga (1990), Sáez et al. (1996), Leistel et al. (1998), Carvalho et al. (1999), and Tornos (2006).

The overall stratigraphic succession is fairly simple and includes a thick (>2000 m) basal siliciclastic sequence made up of shale and quartz arenite deposited on a stable platform, which constitutes the PQ Group of Late Devonian (Givetian-Fammenian) age. The transition to the overlying Volcanic Sedimentary Complex (VS Complex; latest Devonian to middle Visean) is defined by a discontinuous and highly variable unit composed of mass flows, carbonate reefs, and continental sediments that together mark the onset of the pull-apart basin and its irregular deepening (Moreno et al. 1996). The basin now occupied by the IPB is filled with a heterogeneous sequence that includes shale, calc-alkaline andesite to rhyolite, and minor alkaline to tholeiitic basalt. The basalt occurs as submarine flows and dykes and sills, whereas the more felsic volcanic rocks form large (crypto-) domes, sills, and a variety of volcaniclastic sediments (Thieblemont et al. 1998; Tornos 2006; Rosa et al. 2010; Valenzuela et al. 2011b). Near the top of the sequence is a marker level composed of purple shale with abundant jasper and manganese-rich lenses. The VS Complex is capped by foreland-related turbidite deposits of the Baixo Alentejo Flysch Group (Oliveira 1990; Moreno 1993) that record the progradation of the orogenic front above the South Portuguese Zone.

The massive sulphides of the IPB occur in two different settings (Tornos 2006). Those located in the southern part of the belt, where shale predominates over volcanic rocks, are of latest Devonian age (Late Fammenian; Pereira et al. 1996, 2008; Gonzalez et al. 2002) and are situated near the contact of the PQ Group and the VS Complex, or just above the older felsic domes. These sulphide deposits are interpreted as being mainly exhalative, having formed in anoxic bottom waters, probably related to the geological crisis that took place at the Devonian-Carboniferous boundary (Menor et al. 2010). The deposits in the northern part of the belt are younger (Early Tournaisian), and predominantly form replacements of the glassy/porous rocks in the apical or lateral parts of dacitic to

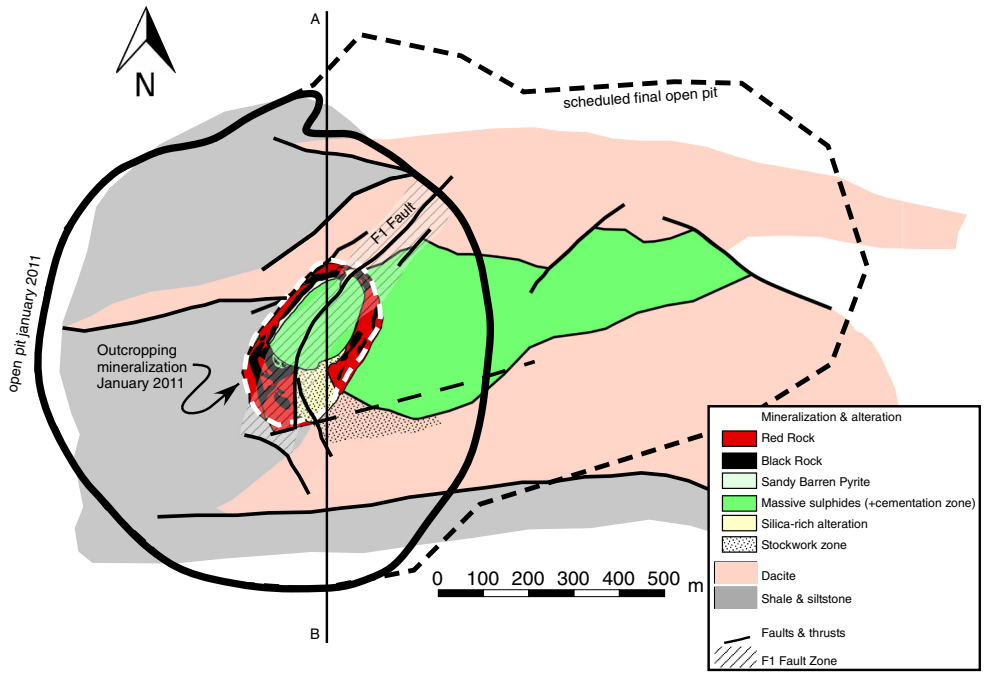

Fig. 2 Pre-Tertiary geology of the Las Cruces orebody. Geology of the open pit (first phase) is based on Miguelez et al. (2011); that of the unexposed zones is based on data from drill cores prior to 1997. *Line A-B* is the approximate location of cross section shown in Fig. 3

rhyolitic domes (Tornos 2006; Valenzuela et al. 2011a). Most of the massive sulphides have an underlying stockwork associated with a well-developed hydrothermal alteration zone that includes both chlorite-quartz and sericite-rich zones. The entire sequence has been affected by lower greenschist-facies regional metamorphism and thin-skinned deformation of Variscan age (Late Visean–Late Moscovian), the latter having formed southward verging recumbent folds and thrust faults.

Outcropping VMS deposits in the IPB are covered by thick gossan caps that have been mined for precious metals since

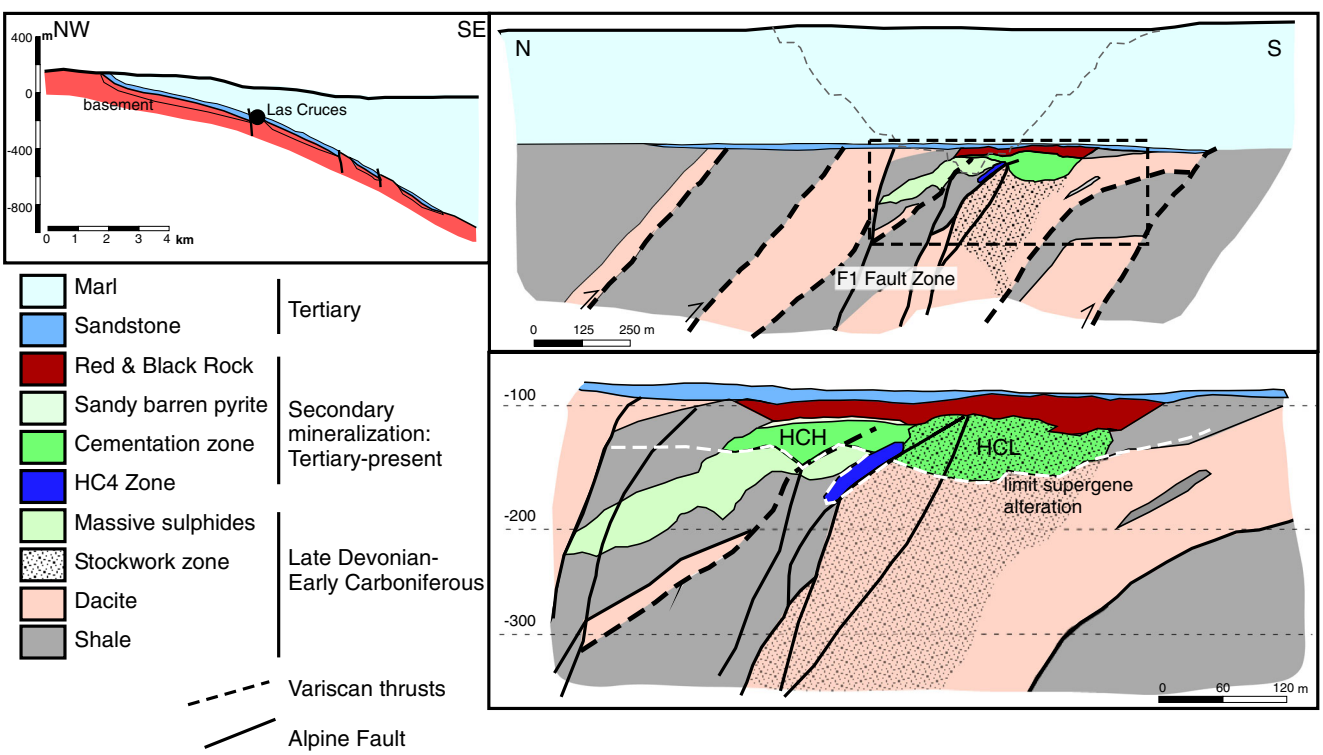

Fig. 3 N-S cross section of Las Cruces orebody, based on surface geology in the open pit and drill core intersections. Regional section (*insert*) is modified from Scheiber et al. (2015). *HCH* and *HCL* refer, following mine terminology, to cementation zones developed on the massive sulphides (high copper high) and stockwork zone (high copper low), respectively

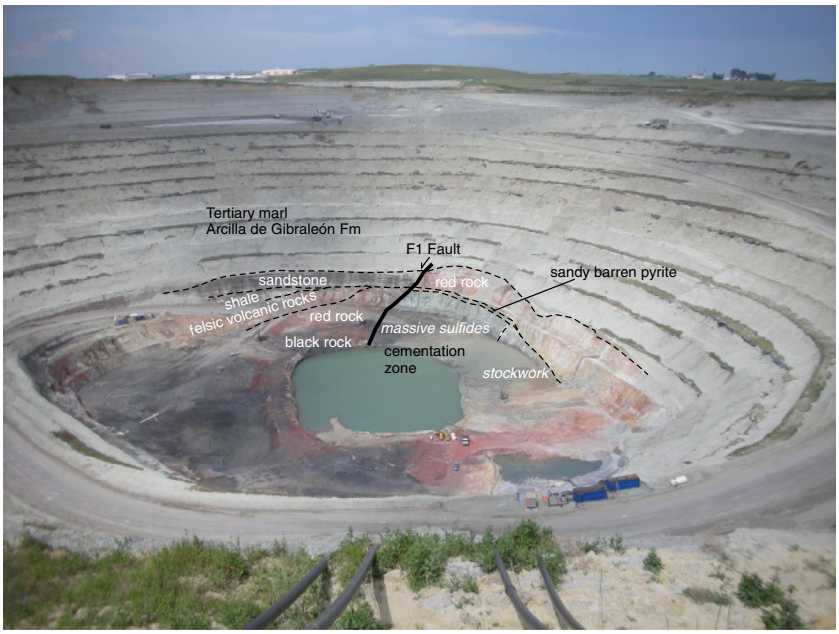

Fig. 4 Photograph of Las Cruces open pit (phase 1—May 2011) showing relationships between the Biogenic Zone (red and black rocks), underlying Cementation Zone, and overlying cap of Tertiary marl

before Roman times but presently only a few remnants are preserved. The most significant ones, at Rio Tinto, Tharsis, and San Miguel, have been described in detail in the recent review of Velasco et al. (2013). In brief, these subaerial gossan caps are up to 100 m thick and are dominated by goethite and hematite with lesser amounts of lepidocrocite, quartz, and jarosite but lack copper oxides, phosphates, silicates, or carbonates, thus suggesting they are mature systems (see Anderson 1982; Scott et al. 2001). As a whole, relative to the primary massive sulphides, the gossans form typical iron caps containing anomalous contents of Ba, Pb (up to 1.2 %), Sb, Bi, As, Sb, Hg, Ag, and Au; systematic depletions are shown by Cu and Zn. Thus, these gossans follow the classical models described by Anderson (1982) with enrichment of residual elements (Ague and Brimhall 1989). There is widespread evidence of lead enrichment in the form of cerussite, anglesite, beudantite, plumbojarosite, or mimetite (Williams 1934; Viñals et al. 1995; Oliveira et al. 1998; Velasco et al. 2013); the As and Sb are mainly hosted in jarosite or stibiconite-bindheimite (Viñals et al. 1995). Silver resides chiefly in iodargyrite and chlorargyrite. All of the other enriched elements are included as nanoinclusions or in the lattice of goethite or jarosite. Gold is predominantly invisible and only locally discrete grains of gold are observed. The base of the gossans in places includes a meter-thick, pale brown to yellow layer enriched in quartz, jarosite, beudantite, and cerussite (Velasco et al. 2013). Here, the metal upgrading (except for Fe) is significant, which promoted early mining of this zone by Romans.

The gossans are interpreted as having formed during Miocene times in a warm, near subtropical climate with short periods of strong seasonal rainfall (Kosakevitch et al. 1993). Beneath the gossans is a small and discontinuous cementation zone dominated by chalcocite and covellite (Almodovar et al. 1997). The cementation zone is at most a few meters thick and only locally, near the faults, extends to depths of 30–40 m below the surface (Williams 1934). The thickness of the cementation zone may have been due to the presence of a shallow water table during oxidation of the primary massive sulphides.

The zone of secondary alteration at Las Cruces differs from that of other deposits in the IPB and elsewhere (Taylor 2011). Only the concealed massive sulphide orebodies of Lagoa Salgada and Gavião, also buried below Tertiary marls, have somewhat similar secondary zones (Relvas 1991; Oliveira et al. 2011). However, both of these deposits have a goethite zone and display widespread acid alteration of the host rocks, but lack the complex secondary assemblages found at Las Cruces.

Geology of Las Cruces deposit

The Las Cruces deposit is located beneath Cenozoic sediments of the ENE-WSW-trending Guadalquivir Basin. The Guadalquivir Basin, the southernmost foreland basin of the Alpine Belt lying between the passive Iberian Massif foreland to the north and the Betic Cordillera to the south (Fig. 1), developed during Neogene compression between Africa and Eurasia. The formation of the basin ended in the Messinian (7.2–5.3 Ma) when it was filled by marine sediments (Sáenz de Galdeano and Vera 1992). The northeast edge of the Guadalquivir Basin is characterized by a set of ENE-WSW- to E-W-trending, steeply dipping (>75°) normal and reverse faults, which are spaced between 300 and 100 m and show a staircase geometry (Figs. 1 and 3). This faulting produced a

rapid deepening of the basement until an approximate depth of 1500 m was attained. At the mine site, the basement is located at a depth of ca. 150–200 m.

Cenozoic sediments

The Cenozoic sequence is a monotonous unit of poorly stratified, bluish to grey, shallow marine marl of Messinian age (Arcilla de Gibraleón Formation; Civis et al. 1987) that increases in thickness towards the southeast. This marl is composed mainly of montmorillonite and disordered kaolinite, with lesser calcite, clinochlore, and quartz, and minor framboidal pyrite. These Tertiary deposits are dissected by Quaternary fluvial sediments.

The base of the sequence is dominated by heterogeneous detrital rocks grouped into the so-called Basal Transgressive Miocene unit, which is not present everywhere. At a regional scale, this unit chiefly comprises bioclastic calcarenite and sandstone-microconglomerate. At the mine site and unconformably above the basement, it contains abundant but irregularly shaped lenses, up to 3–5 m thick, of massive conglomerate with subrounded clasts (1–30 cm) supported by a sandstone matrix; these lenses are interpreted as paleochannels. The conglomerate is heterolithic and includes subrounded fragments of shale, sandstone, quartz, and felsic volcanic rocks derived from the basement; locally present are angular fragments with little evidence of reworking, which are here interpreted as breccias related to fault scarps. Of special interest is the presence of red and porous crumbly fragments up to 1 m in diameter that likely are derived by the erosion of a former and nearby gossan. In places, both the sandstone and the conglomerate show irregular cementation by oosparite and coarse-grained siderite.

The conglomerate is overlain by the sandstone-microconglomerate that shows widespread graded bedding. This unit is up to 10–12 m thick and has the same composition as the conglomerate, but also includes rounded to angular fragments of the bioclastic calcarenite; the groundmass includes quartz, irregularly sericitized plagioclase, K-feldspar, chlorite, and undetermined clay minerals irregularly cemented by oosparite and locally by glauconite; and leucoxene, zircon, and rutile are trace minerals. The micropaleontological study of Moreno et al. (2003) shows that the sandstone is of Late Tortonian age, in broad agreement with the K-Ar age of 6.7 ±0.3 Ma for the glauconite in the groundmass of the sandstone (Galán et al. 1995). The distribution of these detrital rocks displays a major structural control (Fig. 3) and they are in places absent, such that the marl directly overlies the basement.

Regionally, these detrital rocks host a 1–3-m-thick confined porous aquifer (Niebla-Posadas Aquifer). In the mine, this aquifer also saturates the black and red rocks. The Niebla-Posadas aquifer is among the major aquifers in the area and is recharged by rainwater ca. 6 km to the northwest along the basement-cover unconformity (IGME 1983; Scheiber et al. 2015). Groundwater here is a calcium or sodic bicarbonate type, SO_4-rich but Cl-poor, alkaline (pH ≈ 8.0), and has outflow temperatures between 18 and 31 °C (Table 2); a gradual depletion in free oxygen and mixing with deep fluids is shown from the recharge zone to the Las Cruces mine. The high pH and low salinity limit this groundwater to very low metal contents except As. Within the detrital rocks and beneath the marl, which has very low transmissivities, are accumulations of sour gas (Melendez-Hevia and Alvarez del Buergo E 1996).

The host Paleozoic sequence

The pre-Miocene paleosurface is planar and gently dips to the south. Rocks beneath this surface show a strong subaerial alteration, expressed by the presence of thick paleosols at a regional scale.

The host strata of the Las Cruces deposit have an average strike of N90°E and variable dips between 20 and 45°N (Doyle 1996). Cleavage dips 60–80°N, suggesting that the deposit is on the northern limb of an antiformal structure, a location similar to those of many deposits of the IPB because the inverse limbs are systematically disrupted by shear zones (Quesada 1998). The Las Cruces massive sulphide lens is situated in the same stratigraphic interval as the nearby Aznalcóllar and Los Frailes deposits (Conde et al. 2003), ca. 12.5 km to the west (Fig. 1). Here, the VS Complex includes massive volcanic rocks (domes and sills), and volcaniclastic breccia and arenite interbedded with shale and chemical sediments (chert and jasper). Felsic volcanic rocks (dacite and rhyolite) dominate over andesitic and basaltic-andesitic flows and sills (Almodovar et al. 1998; Conde et al. 2003).

The mine sequence comprises four volcanosedimentary units (Conde et al. 2007). The footwall is a heterogeneous dome complex of porphyritic dacite (>300 m thick) with associated in situ and transported hyaloclastite occurring within volcaniclastic aprons; the massive rocks display abundant peperite textures that suggest forceful injection of magma into wet sediments. These rocks are overlain by a sequence ca. 80 m thick dominated by black shale with interbedded crystal-rich volcaniclastic sandstone and volcaniclastic argillite and siltstone. Sulphide mineralization is localized in the footwall of this sequence, along the contact between the dacite and black shale (Fig. 3). Black shale in the footwall of the massive sulphides typically has disrupted centimeter-sized layers of white to grey chert showing parallel lamination (Fig. 5b) that probably correspond to chemical (exhalite) deposits. They are commonly folded and brecciated and locally contain pyrite aggregates up to 2 mm that resemble sulphate crystals—if true, these crystals could either be relicts of former evaporites or hydrothermal anhydrite that precipitated on the seafloor. These rocks also have abundant disseminated pyrite,

Table 2 Synthesis of chemical and isotope data of present-day water in Las Cruces deposit

Aquifer	Composition	Control	*T* °C	pH	TDS	$\delta^{18}O$ ‰	δD ‰	$\delta^{13}C$ ‰	$\delta^{34}S$ ‰	Origin	Notes
Niebla-Posadas (n = 28)	Calcium or sodic bicarbonate, SO_4-rich but Cl-poor	Stratabound confined aquifer	18–31 (24)	6.6–9.4 (8.0)	263–1579 (846) High Ca, Mg	−5.5 to −3.5 (−4.7)	−35 to −17 (−27)	−11.3 to −5.8 (−8.4)	−17 to +20[a]	Modified rainwater	Recharged ca. 6 km NW
Deep reservoir (*n* = 11)	Sodium chloride waters	Upwelling, controlled by major faults	22–43 (38)	6.7–7.9 (7.5)	465–2150 (1380) High Na	−5.8 to −3.8 (−4.8)	−32 to −24 (−29)	−10.7 to −7.6 −8.8		Connate water	Deep marine intrusion? Inherited Miocene waters? Cation exchange?

Error ±2 ‰ in δD and ±0.2 ‰ in $\delta^{18}O$ and $\delta^{13}C$ values. Analysis: IACT Granada. TDS total dissolved solids in mg/l. Average values in parenthesis

[a] Data from Scheiber et al. (2015)

pyrrhotite, and arsenopyrite. The shale in the hanging wall of the massive sulphides contains abundant intercalations of felsic volcaniclastic rocks as well as structures indicative of dewatering; included large clastic dikes disrupt overlying sediments. This shale hosts abundant stratabound to discordant breccia bodies less than 0.5 m thick with 1–2-cm-sized fragments of white hydrothermal quartz; the origin of this rock is unknown.

The hanging wall of the orebody includes a heterogeneous sequence (450-600 m thick) that can be grouped in two major units. The lower one is a thick package of heterogeneous breccia and crystal-rich sandstone that likely formed as debris flows; a single layer containing pumice-rich fragments has been traced over the entire area, including Aznalcóllar and Los Frailes (Conde et al. 2007). The upper unit comprises shale with siltite intercalations and felsic epiclastic rocks. A distinctive massive dacite unit, probably a flow or sill, locally caps these rocks. The age obtained by Barrie et al. (2002) for a hanging wall dacite (354 ± 0.7 Ma) suggests that these late rocks are Early Tournaisian. Chemostratigraphy indicates that the sequence has a calc-alkaline affinity with compositions between basaltic andesite and rhyodacite, with no significant gaps.

The black shale that hosts the massive sulphides is enriched in elements typically present in anoxic settings (e.g., V, Cr, and Mo) whereas the barren shale of the hanging wall has low contents of these elements and was likely deposited under sub-oxic to oxic conditions. These different features support evidence found in other massive sulphide deposits of the IPB that the massive sulphide mineralization formed in local anoxic conditions (Tornos et al. 2008).

The sequence hosting the massive sulphides shows major deformational features that are especially intense near the massive sulphides with deformation being preferentially channeled within the black shale.

The Paleozoic rocks host a second fluid reservoir from where overpressured waters presently flow upward along faults (Fig. 3). Water in this deep reservoir is chemically different but isotopically similar to that of the Niebla-Posadas aquifer (Table 2). These are also alkaline (pH ≈ 7.5), reduced, sodium chloride waters with variable CO_2 and low contents of Ca, Mg, and SO_4; this water is ca. 3× more saline than that of the Niebla-Posadas aquifer (Table 2). Before mining, this overpressured water flowed at surface temperatures above 40 °C (Knight 2000); the current temperature is between 22 and 43 °C. However, application of silica and Na/K chemical geothermometers (Henley et al. 1984) suggests temperatures of equilibrium for this water (upub. data) as high as 95 °C. The ultimate origin of this water is unknown; the salinity and geochemical signature are similar to those of seawater. However, oxygen and hydrogen isotope values are close to those of the regional groundwater (Table 2 and ESM Table 1), suggesting that this could correspond to rainwater that has leached

evaporites from the Tertiary sequence. At the mine scale, there is abundant evidence of mixing between the two water end-members (Scheiber et al. 2015). Significantly, no methane has been found in the Niebla-Posadas aquifer or the deep reservoir.

Primary sulphide mineralization

The primary orebody at Las Cruces forms a single, large, massive sulphide lens with minimum dimensions of ca. 1000 m long, 500 m down dip, and between 30 and 130 m thick. Average dips are near 25–45°N, but in the currently mined open pit, the dip increases significantly up to 50°N due to effects of several imbricate faults (Fig. 3). To the west, the sulphide mineralization thickens and is truncated by a N-S fault; the primary massive sulphide deposit is open at depth and to the northeast (Doyle 1996; Knight 2000). This deposit is underlain by a large stockwork zone of unknown extent, accompanied by related hydrothermal alteration that affects the footwall dacite and shale (Doyle 1996).

The massive sulphides

The primary massive sulphides show a distinctive metal zoning (Doyle et al. 2003) characterized by an upper Zn-rich zone and a lower Cu-rich zone. These ore zones are interbedded with barren massive pyrite, which is located mainly in the central part of the lens. The mineral assemblage is similar to that of the other similar deposits of the IPB, and includes predominant pyrite and subordinate chalcopyrite, sphalerite, and galena and traces of tetrahedrite-tennantite, Bi-Pb sulphosalts, bismuthinite, stannite-kesterite, and cassiterite, together with quartz, barite, siderite, Ba-bearing sericite, and chlorite, and traces of rutile and zircon (Knight 2000; Blake 2008). Euhedral arsenopyrite is fairly common, occurring especially near or within the hosting black shale. Blake (2008) described the presence of abundant enargite and covellite but these minerals are here interpreted as secondary.

The massive sulphides show a conspicuous layering. Few clear sedimentary features can be observed, which include banding and graded bedding, especially visible in interbedded shale and chert. Within the copper-rich zones, paragenetically early pyrite forms aggregates of minute framboids (<20 μm) with interstitial pyrrhotite, and is partially recrystallized to small (<30 μm) euhedral crystals with few inclusions. It is cemented by a widespread, fine-grained, porous pyrite intergrown with chalcopyrite. Voids are commonly infilled with sphalerite and minor galena and tetrahedrite, and lined with botryoidal pyrite. Also the sulphides present abundant colloform and circular-like structures, as well as a continuous layering that show fibrous growth. These late sulphides are here interpreted as due to replacement of poorly ordered sulphides, with the observed textures likely related to microbial activity. These early assemblages are brecciated, forming a rock with angular to subrounded fragments millimeters to several centimeters in diameter, cemented by massive chalcopyrite. A second event that produced coarse-grained chalcopyrite and galena cuts all older assemblages.

The polymetallic zones contain centimeter-thick bands of alternating pyrite + chalcopyrite and sphalerite + chalcopyrite + galena. The sulphides other than pyrite show widespread recrystallization to a granoblastic assemblage hosting abundant rains of minute subhedral pyrite. The sphalerite is iron-

Fig. 5 Selected photographs of mineralization at Las Cruces. **a** Massive sulphides hosting irregular remnants of hydrothermally altered dacite, suggesting that part of the massive sulphides replaced the footwall volcanic rocks; NE zone phase 1 open pit. **b** Siltstone with intercalations of chert in footwall of massive sulphides, showing crystals of former sulphates replaced by pyrite. Width of photograph 5 cm. **c** Resedimented stratiform mineralization of uppermost massive sulphide showing clasts of sulphides and sandstone (**c**) as well as soft clasts of shale. Width of photograph 5 cm. **d** Veins of the Advanced Cementation Zone showing open-space filling of massive, steely chalcocite (*cc vein*) cutting massive sulphides with some replacement by sooty chalcocite (*cc repl*). Veins are located near the F1 fault. High-grade zone of the second phase; width of photograph 20 cm. **e** Chalcocite vein with early pyrite, chalcopyrite, and bornite replaced by chalcocite. Sample LCT-4; width of photomicrograph (*reflected light*) 1.8 mm. **f** Chalcocite vein with early chalcocite destabilized to low chalcocite, anilite, and digenite and cut by veins of late chalcocite; primary pyrite in selvage (*top*) is also irregularly replaced by an intergrowth of chalcocite, enargite and digenite. Sample FP-FT-727; width of photomicrograph (*reflected light*) 1.8 mm. **g** Early enargite (*en*) replaced by later chalcocite (*cc*) corroding pyrite (*py*). Sample LCT-4; width of photomicrograph (*reflected light*) 1.8 mm. **h** HC4 ore with veinlets of covellite in primary massive sulphides (sphalerite and galena). Drillhole CR-427 165.9 m; width of photograph (4 cm). **i** Overview of the zone of acid alteration on dacite beneath the massive sulphides; phase 2. *T*: Tertiary sediments; *G*: Gossan and red and black rocks; *MS*: massive sulphides including the cementation zone; *AA*: Dacite with stockwork and superimposed acid alteration. **j** Detail of the hydrothermally altered dacite replaced by kaolinite with disseminated and vein-like pyrite inherited from primary VMS stockwork, cut by veins of massive alunite; sample LCT-98. *Coin* is 2.5 cm in diameter. (**k**) Subvertical epithermal vein cutting massive sulphides. Vein shows banded structure with low-temperature quartz (*Q*), barite (*ba*), and sulphides (mainly pyrite and chalcocite (*cc*)) replaced by late barren calcite (*cc*). Assemblage includes pyrite (*py II*) growing in vein center or its selvage on earlier primary pyrite (*py I*) of massive sulphides. Sample LCT-13; width of photograph 4 cm. **l** Epithermal vein showing remnants of likely dissolved calcite in quartz and pyrite. NE side of open pit; phase 2. Width of photograph 5 cm. **m** Red rock, containing siderite and galena (*gn*) and exotic clasts of volcanic rocks (*cl*) inherited from former gossan. Sample LCM-13. Phase 1 open pit. Width of photograph 6 cm. **n** Black rock with iron monosulphides (mainly greigite, FeS) coated by galena (*gn*) in calcite. *Arrow* marks laminae of fine-grained galena interpreted as former microbial mats. Sample LCT-2b. Width of photomicrograph (*reflect light*) 1.8 mm. **o** Late sulphides, including chalcopyrite (*cp*), bornite (*bn*), and enargite (*en*) coating open fractures and breccias. These late veins postdate the precipitation of chalcocite (*cc*) of the Advanced Cementation Zone. Width of photograph 6 cm. **p** Late coatings of chalcedony in brecciated massive sulphides. Width of photograph 4 cm

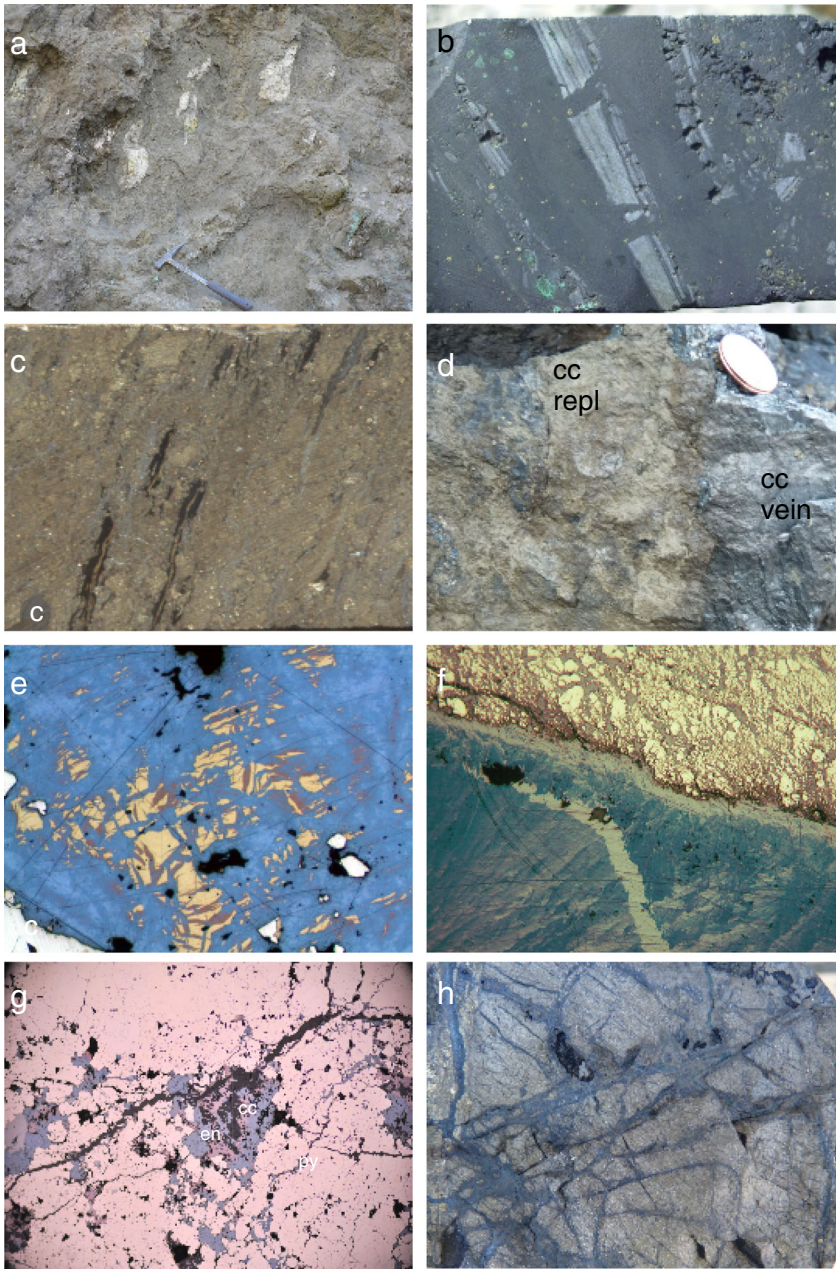

poor ($Zn_{48\text{-}50}$ $Fe_{0.4\text{-}1.3}$ $S_{49\text{-}51}$) and displays abundant evidence of late replacement by chalcopyrite, including the presence of chalcopyrite disease and replacements along veins and grain edges. These textures suggest widespread hydrothermal refining with replacement of the early sphalerite-galena by late chalcopyrite via hotter hydrothermal fluids (Large 1992). Locally, concentric zones, some millimeters to 1 cm in diameter, have an internal zone composed of sphalerite and an outer rim of chalcopyrite; these are interpreted as fluid conduits. The sphalerite and chalcopyrite contain inclusions of tetrahedrite-tennantite that show widespread As-Sb substitution (Blake 2008). Also present are abundant wittichenite and more rare minerals of the aikinite-bismuthinite series occurring in small (<25 μm) grains intergrown with galena and bismuthinite, and hosted by chalcopyrite. Cassiterite forms minute sub-euhedral crystals, 3–10 μm in diameter, enclosed by the sphalerite and chalcopyrite.

Widespread late recrystallization has masked most of the primary features, leading to the formation of coarse (>500 μm) euhedral to sub-euhedral aggregates of sulphides. Deformation is responsible for the formation of alternating layers of sphalerite-chalcopyrite-galena and pyrite.

While the uppermost shale-hosted massive sulphides seem to be exhalative, the lowermost orebody seems to have been formed mainly by replacement. Evidence of replacement includes the presence of relicts of variably altered dacite within the massive sulphides (Fig. 5a) and of a gradual contact with the underlying stockwork mineralized zone. No oxidation has

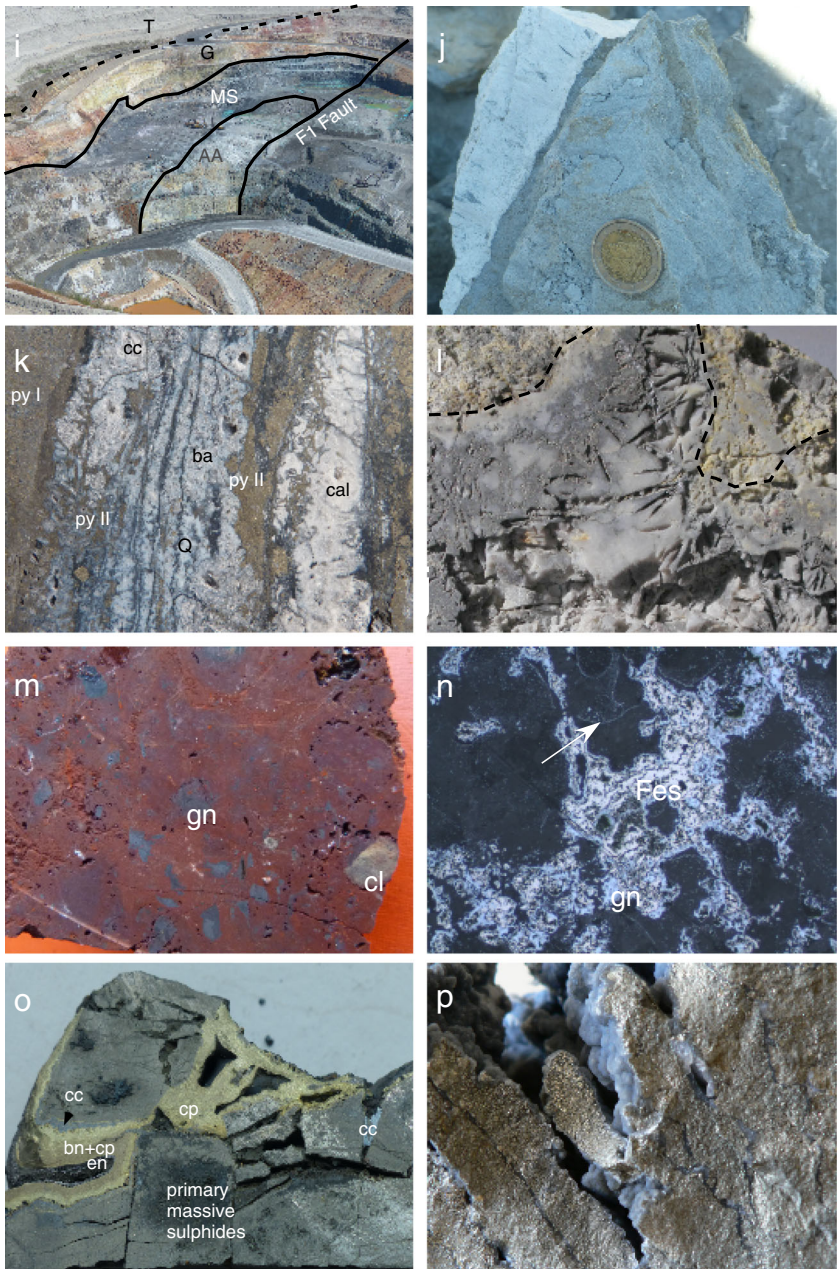

Fig. 5 (continued)

been observed in the hanging wall of the massive sulphides, thus indicating that seafloor oxidation processes were minimal and that the massive sulphides were originally isolated from an oxic open ocean.

The stockwork zone and related hydrothermal alteration

A large Cu-rich stockwork zone can be traced ca. 200 m beneath the massive sulphides. This stockwork zone is hosted by hyaloclastitic dacite and shale with chlorite ± quartz alteration, and is bordered by a large sericite + quartz ± siderite zone of unknown extent. Veins of the stockwork, between 0.5 and 2 cm thick, are folded or subparallel to the regional cleavage and contain quartz, siderite, and chlorite with variable amounts of pyrite and chalcopyrite, and only sparse sphalerite and galena.

The structure of the primary mineralization is similar to that of other massive sulphide deposits of the IPB. Contacts of the massive sulphides have channelized the Variscan deformation, leading to the development of ramp and flat structures (Silva et al. 1990; Tornos et al. 1998; Onezime et al. 2002) that include tectonic duplexes of massive sulphides, shale, and felsic volcanic rocks bounded by cataclasite; locally, the stockwork is thrust above the massive sulphides.

Secondary mineralization and alteration related to the paleosurface

Occurring between the primary mineralization and the Tertiary sediments is a discontinuous, flat-lying lens of secondary mineralization having an approximate extent of 0.4 km^2 (Figs. 2 and 3). This zone of secondary alteration has a poorly defined vertical zonation that broadly includes the following, from top to bottom: (a) the red rock (0–20 m); (b) black rock (0–5 m); (c) discontinuous lenses of massive to sandy silica (<5 m), predominantly located lateral to the red rock or within the red and black rocks; (d) the sandy barren pyrite zone (2–3 m); and (e) the cementation zone (Fig. 4). The complete section is only rarely present, however, and in places the sandy barren pyrite zone is directly below the Tertiary sandstone. As a whole, the red and black rocks contain high concentrations of Pb (up to 20 wt%), Ba (up to several percent), Sn (up to 1 wt%) Bi (up to 1500 μg/g), As (up to 5760 μg/g), Hg (up to 1180 μg/g), Sb (up to 5500 μg/g), Ag (up to 1340 g/t), and Au (up to 350 g/t), and uniformly low Cu and Zn (ESM Table 2 and Yesares et al. 2014). The red and black rocks have low Al contents and only traces of clays. Thus, they show the same pattern of metal enrichment as the gossans in the IPB (Velasco et al. 2013). Lead-rich rocks invariably have high contents of precious metals but the inverse is not always true.

Beneath the red and black rocks, it is the cementation zone that has a broadly stratabound character and forms an irregular discontinuous blanket on top of the massive sulphides (Fig. 3). The thickness of this zone is between 10 and 40 m (avg. 20 m), but near faults, there is secondary mineralization that extends to depths of 80 m below the paleosurface. The entire sequence, except the red rock, is cut by subvertical veins and breccia bodies.

Of major importance here is the presence of an array of faults that control the location and grade of the secondary mineralization (Figs. 2, 3, and 4). The most significant, termed the F1 fault, has a N-S trend in the southern part of the open pit but bends to a NE-SW strike in the northeast part, implying an *en echelon* morphology (Fig. 2); it dips 60 to 80°W and shows a strike-slip normal displacement. The trace of the F1 fault marks zone of high-grade secondary ores as well as zones of major development of the red and black rocks, suggesting that this fault controlled fluid flow during formation of the secondary mineralization; as noted above, this fault currently channelizes water in a major aquifer. The width of the fault is highly variable but locally includes a fault breccia up to 3 m thick composed of heterolithic fragments in fault gouge. This breccia has an associated network of fractures that extends up to 50 m on both sides of the fault but is especially well developed in the lower (W) block. The F1 fault cuts the basement rocks but gradually diminishes within the Tertiary sediments (Fig. 4). Significantly, the Tertiary conglomerate is not present on the eastern side of the fault, and the sandstone layers have different thickness on both sides, thus indicating that the fault was active at least until Tortonian time. The orientation of this fault differs from that of regional Variscan structures having dominant WNW-ESE trends and north dips (Quesada 1998). Our interpretation is that this fault system postdates the Variscan deformation and very likely is one of the Alpine structures that formed during opening of the basin, the trend being consistent with a transfer fault that formed between the dominant Alpine WNW-ESE faults (Fig. 2) during a period of sinistral, strike-slip movement.

The remnant gossan

The few existing remnants of the primary gossan are dominated by an earthy ochre to brownish rock containing breccias made up of fragments of quartz and host rocks supported by a groundmass of goethite, hematite, and minerals of the jarosite group, together with accessory barite, cerussite, and anglesite and traces of native copper, smithsonite, minium, and massicot; Blake (2008) also reported pyromorphite and mimetite. The upper contact is extremely irregular, with variably sized fragments of gossan occurring in the unconformably overlying sediments. In places are zones (possible karst-like cavities) rich in nontronite and alunite. The gossan also contains relatively abundant cassiterite, zircon, apatite, and rutile disseminated in layers, which likely are inherited from erosion of the former massive sulphides and subsequent concentration as detrital grains. The lowermost part of the gossan hosts an ochre-colored rock composed of fine-grained quartz with abundant hematite, jarosite, and beudantite that is very similar to the basal jarosite-rich zone of other gossans in the IPB.

In most previous studies of the Las Cruces deposit, all of the rocks capping the cementation zone have been grouped as gossan. As discussed below, these rocks contain an assemblage very different from that of the gossans and, thus, this widely used term is misleading. Use of the term gossan should be restricted to oxidized ferruginous rocks that occur above sulphide-bearing deposits (Boyle 2003; Taylor 2011; Velasco et al. 2013).

The red rock

The red rock has a distinctive ochre to reddish color and records nearly complete replacement of the earlier (primary) gossan (Figs. 4 and 5m). The red rock has a chaotic internal structure with alternating zones of different colors and porosities (Yesares et al. 2014) with most of its structure inherited from the primary gossan. Within large zones, especially in the lower part of the red rock, the gossan is irregularly replaced by an assemblage of siderite and galena, but with original proportions of barite and quartz. The siderite has replaced

hematite and goethite via a network of veinlets or through sharp replacive fronts. Siderite is accompanied by fine-grained aggregates of skeletal galena that form aggregates less than 1 cm in diameter intergrown with coarse-grained siderite (Fig. 5m). Locally within these rocks are millimeter-thick veinlets composed of iron monosulphides and small amounts of silver sulphides and sulphosalts, similar to those that occur widely in the black rock. Yesares et al. (2014) have described alternating siderite and goethite bands that suggest the precipitation of these minerals took place under variable redox conditions.

The black rock

The black rock forms a discontinuous layer, predominantly in the contact between the red rock and underlying massive sulphides (Fig. 3). It was found mainly in the western part of the F1 fault, which was the first zone to be mined (Fig. 4). However, the black rock is much scarcer in other parts of the mine. The black rock is equivalent to the black Gossan of Knight (2000) and the Galena-rich Layer of Blake (2008).

The black rock contains nearly monomineralic, subhorizontal layers of massive fine-grained galena variably intergrown with iron sulphides, coarse-grained calcite and fine-grained quartz or their mixtures. The black rock includes minor barite, quartz, and nontronite, and traces of Ag-bearing tetrahedrite-tennantite, cinnabar, cassiterite, native silver, and silver- and lead-bearing sulphides and sulphosalts like acanthite, sternbergite, proustite-xanthoconite, pyrargyrite, pearceite, and jamesonite. Blake (2008) also reported the presence of bismuthinite, possible boulangerite, argentopyrite, aramoyaite, cannfieldite, native bismuth, and arsenic as well as other undetermined As-Sb-Bi-bearing phases; Yesares et al. (2014) described imiterite and miargyrite. The iron monosulphides occur in irregular ferromagnetic patches as minute (1–3 μm) framboidal aggregates of isotropic greigite enclosed in euhedral smythite crystals, and in later marcasite and pyrite (Fig. 5n). The galena forms younger aggregates of fine-grained (3–5 μm) framboids, radiating and skeletal aggregates that postdate the iron monosulphides, and intergrowths with calcite, barite, and quartz. Locally, there is evidence of replacement and pseudomorphing by galena of preexisting supergene lead-bearing minerals such as anglesite, cerussite, mimetite, and pyromorphite. The black rock contains structures that in SEM images resemble fossils of prokaryotes that are made of galena and fixed on calcite (Tornos et al. 2014). They are ca. 5–10 μm long and ≤1 μm wide, and comprise unbranched and twisted, threadlike aggregates without external morphological features. This suggests that the galena precipitated as an extracellular coating of prokaryotes (Tornos et al. 2014). These structures are similar to microbial filamentous structures reported elsewhere (Rasmussen 2000; Grenne and Slack 2003). Furthermore, the black rock shows convoluted chemotaxic textures with films of fine-grained galena hosted by calcite that resemble biofilms (Fig. 5n). However, these inferred microfossils are only rarely found; most of the galena occurs as skeletal crystals. Our interpretation is that the majority of these skeletal crystals formed from the maturation of early bacteriomorphs. Thin (<1 mm) fractures coated with large platy crystals of secondary galena cut the overlying sandstone and marl (Yesares et al. 2011a), showing that this mineralization postdates burial. Veinlets with similar assemblages are found in the underlying rocks, including the sandy barren pyrite zone, the cementation zone, and even the primary massive sulphides (Knight 2000). The silver-bearing minerals chiefly occur intergrown with iron sulphides, but also in dissolution cavities within galena and calcite. Gold also occurs in the black rock where it forms Au-Ag-Hg alloys with highly variable compositions between native gold and electrum (Blake 2008; Yesares et al. 2014); amalgam and auricupride are also present.

The black rock replaced the red rock and fragments of the Miocene conglomerate via a gradual increase in proportions of galena, replacement of siderite by calcite, and recrystallization of quartz. The lower contact is gradual and characterized by rims, replacement, and cementation of the sandy pyrite by a mixture of fine-grained galena, iron monosulphides, and silver-bearing minerals.

The black rock rapidly weathers during mining, which probably caused Yesares et al. (2014, 2015) to interpret it as a mylonitized and altered layer of black shale that bounds a major subhorizontal thrust fault located between the red rock and the sandy barren pyrite. In their model, this fault controlled the formation of the mineralization due to changes in redox conditions. However, our interpretation of the chemical and mineralogical compositions is more consistent with the black rock having formed by sulphidization and carbonatization of the gossan (Tornos et al. 2013, 2014), from which it inherited the geochemistry and resistate minerals; in fact, this black rock is sometimes made up of massive galena and shows replacive contacts with the red rock. Mapping shows that it forms subhorizontal bodies totally different from the steeply dipping grey shale that caps the massive sulphides in the southern part of the open pit (Fig. 2).

The sandy barren pyrite zone

Capping the cementation zone rock is a continuous, 2- to 3-m-thick layer of sandy, coarse-grained pyrite that typically is overlain by the red and black rocks but locally is directly below the Tertiary sediments. This pyritic rock is poor in base and precious metals, having only low (<0.1 %) Cu grades and virtually no Zn (ESM Table 2). It comprises poorly cemented, 40–2000-μm anhedral grains of pyrite with only local inclusions of chalcopyrite and sphalerite, and remnants of almost completely dissolved intergranular chalcocite. The pyrite

grains are similar to the coarse-grained pyrite found in the massive sulphides, and thus are interpreted as being the product of diagenetic/metamorphic recrystallization of early pyrite. The pyritic rock is clearly replaced by the black rock, as galena coats and replaces the pyrite crystals. The contact with the underlying cementation zone is sharp and marked by a distinct Cu-rich zone made up of dusty chalcocite or pyrite coated with chalcocite.

Our interpretation of the sandy barren pyrite zone is that it represents a zone of massive sulphides that has been leached of the more soluble sulphides (sphalerite, galena, and chalcopyrite), during accelerated evolution of a supergene profile due to a rapid drop of the water table; here, the velocity of acid leaching is faster than that of oxidation, thus leaving a zone of barren pyrite. Similar rocks have been described in the uppermost part of cementation zones in other sulphide deposits (Belogub et al. 2008; Velasco et al. 2013).

The cementation zone

The large cementation zone at Las Cruces includes abundant chalcocite and is the only ore currently mined for copper. Most of this secondary mineralization has irregularly replaced the original primary sulphides in a pattern typical of cementation zones described elsewhere (Emmons 1918; Brimhall et al. 1985; Ague and Brimhall 1989; Sillitoe 2005; Braxton et al. 2009). In general, the copper enrichment in the cementation zone is ca. 5× that of the protore (Titley and Beane 1981), but in Las Cruces is up to 20× in high-grade zones, yielding average grades higher than that of any other deposit. This is due to the presence of a high-grade ore (advanced cementation zone) superimposed on a conventional cementation zone.

The conventional cementation zone is volumetrically dominant (>80 vol% ore) and is characterized by relatively low copper grades (<5 % Cu). It displays classical supergene copper enrichment with the secondary sulphides replacing most of the base-metal sulphides (chalcopyrite, sphalerite, and galena), and to a lesser extent the pyrite. The advanced cementation zone is located in a corridor some tens of meters wide adjacent to the F1 fault system. Despite its relatively small volume (2.35 Mt), this zone includes high-grade ore, where in mine blocks have grades between 10 and 20 % leachable Cu; the average grade is 13.2 % Cu. The most characteristic feature of this ore is the presence of 1-cm to 0.5-m-thick veins of massive steely chalcocite (Fig. 5e) that are sub-parallel to the fault and cut the massive sulphides. These veins are irregularly enclosed within breccia ore in which the secondary copper minerals occur in fractured pyrite and coat abundant but minute fractures less than 0.2 mm thick. Also present locally are stratabound masses of powdery and crumbly, black, sooty chalcocite grains 0.1–0.2 mm in size interpreted as former massive base-metal sulphides that have been completely replaced. These rocks inherit the structure of the protolith and contain abundant cavities of dissolved pyrite crystals. The veins, massive replacements, and breccia ore are grouped into the high copper high density (HCH) in mine terminology. Borders between the cementation zone and the advanced cementation zone are gradual. Furthermore, the borders include zones of primary massive sulphides with no evidence of supergene modification. Gradually, the grade of the leachable ore diminishes downwards into the primary massive sulphides. Despite being pervasively altered (see below), host rocks other than the stockwork zone do not carry economic mineralization.

The cementation ore developed on the primary stockwork zone is somewhat different from that formed on the massive sulphides, being probably related to the presence of reactive silicates. This has been observed in supergene alteration zones of porphyry copper systems, where secondary copper sulphides not only replace pyrite but also silicates such as chlorite and feldspar that are able to buffer the pH of the descending acidic waters (Brimhall et al. 1985; Ague and Brimhall 1989; Sillitoe 2005). Here, the primary and folded quartz-rich veins of the stockwork are leached of sulphides other than pyrite; the supergene chalcocite forms coatings or replacements as predominantly powdery copper sulphides, giving rise to the so-called HCL (high copper low density) ore of the mine.

The mineral assemblage of the cementation zone is complex (see also Yesares et al 2015) but mainly comprises minerals of the chalcocite group. They coexist with lesser amounts of bornite, chalcopyrite, pyrite, enargite, tennantite-tetrahedrite (fahlore), and galena. Famatinite has been also reported by Blake (2008). Several of these minerals are uncommon in cementation environments, but their presence within the chalcocite-rich veins at Las Cruces leaves little doubt about their secondary origin.

The veins show a characteristic well-developed zonation. The earliest minerals to precipitate are chalcopyrite ± pyrite, with the chalcopyrite showing abundant flame-like intergrowths and replacements of bornite (Fig. 5f, g); associated there is abundant enargite as relatively large (<200 μm) anhedral grains. Dominant chalcocite replaced all previous minerals; the early chalcocite is made up of intergrown plates of whitish digenite (Cu_9S_5) and pale blue chalcocite (Cu_2S) in small lamellae that are the likely product of low-temperature destabilization of high or hexagonal chalcocite (Rahmdor 1980). The chalcocite is replaced by a complex assemblage that includes early orthorhombic grey chalcocite ss with well-developed exfoliation and intermingled Cu-rich sulphide minerals including enargite, digenite (≈$Cu_{1.94}S$), anilite (Cu_7S_5), and finally djurleite (≈$Cu_{1.97}S$), the most abundant phase. Locally, chalcocite minerals are intermixed with other secondary copper sulphides like yarrowite (≈$Cu_{1.1}S$) and spionkopite (≈$Cu_{1.5}S$—the formerly blaubleibender covellite). However, this dominant sequence is not constant, as late bornite and enargite have been found replacing chalcocite. Both enargite

and bornite are replaced by fahlore with variable As/Sb ratios and up to 13 % Hg (Blake 2008) and a third generation of fine-grained enargite intergrown with the fahlore. Covellite is paragenetically late and scarce in the cementation zone, occurring mainly along the edge of the veins and locally is associated with wittichenite and Ni-bearing sulphides (Knight 2000). Finally, galena can occur as fine-grained aggregates and coatings. Gold and silver contents are negligible within the cementation zone.

Textural and paragenetic relationships are more obscure in the conventional cementation zone. Here, the primary pyrite seems to be replaced by early enargite followed by chalcopyrite, bornite-fahlore, and predominant chalcocite.

Pyrite within the most altered rocks is uniformly recrystallized to coarse (1–3 mm) anhedral to euhedral grains having abundant inclusions of chalcopyrite ± bornite ± enargite. The texture of this pyrite differs from that of primary massive sulphides elsewhere in the southern IPB. Because the hypogene pyrite lacks inclusions of bornite and enargite and contains abundant sphalerite and galena inclusions, our preferred interpretation is that this pyrite is secondary and related to the early stages of secondary alteration, likely accompanied by widespread recrystallization during leaching of the primary base-metal sulphides. Enargite was first described at Las Cruces by Knight (2000) and its presence later confirmed by other workers (Blake 2008; Tornos et al. 2013; Yesares et al. 2014). It forms fine-grained, anisotropic masses that replace the early chalcocite, in places intergrown with chalcopyrite and bornite; the enargite is replaced by later tennantite.

The lowermost orebody (HC4; Fig. 3) includes a lens up to 12 m thick composed of massive covellite replaced by chalcocite; this mineralization has replaced massive sulphides made up of sphalerite and galena in the faulted footwall of the primary orebody (Fig. 5h). Some veins have a well-developed layering (see Fig. 5b of Yesares et al. 2015) that records direct precipitation from fluids in an open space. As a whole, the sequence of the cementation assemblage at Las Cruces defines a zonation similar to that of several other deposits, and is in agreement with conceptual and numerical models (Sato 1960; Alpers and Brimhall 1989) but includes a rather uncommon assemblage of early, low-fS_2 Cu-Fe sulphides as well as phases rich in As-Sb.

The massive sulphides beneath the cementation zone show conspicuous evidence of dissolution in that most sulphides, excluding pyrite, seem to have been dissolved leading to the formation of large zones of crumbly and porous pyrite with 5–10 % vol. vugs. This feature has been widely observed to depths of as much as 400 m beneath the original paleosurface.

Epithermal veins and breccias

The cementation and sandy barren pyrite zones and, to a lesser extent, the red and black rocks are cut by a second set of subvertical veins. These veins locally form sheeted vein systems some tens of wide were individual veins are between 1 and 20 cm thick and are parallel to the major F1 fault system. The sheeted veins sharply cut the deformed stockwork veins, primary banding of the massive sulphides, and veins of the advanced cementation zone.

The veins show a banded, millimeter-thick structure that resembles that of epithermal veins (Fig. 5k, l) and includes different proportions of quartz, barite, calcite, and sulphides. Cockade, banded, and botryoidal textures and vugs infilled with euhedral crystals are common. The earliest assemblages include fine-grained quartz that locally forms euhedral crystals within the vugs. A second stage is represented by chalcedony and barite, the latter only abundant in the upper part of the veins, in places as bladed crystals. Calcite occurs as late infillings and replacements. The sulphides show a paragenetic sequence similar to that of the cementation zone. Pyrite is especially abundant within vein selvages, where it forms isolated euhedral crystals or aggregates coating earlier pyrite (Fig. 5l). This vein-selvage pyrite is replaced by chalcopyrite plus bornite and enargite; the enargite occurs as larger crystals than those in the cementation zone and shows widespread replacement by fahlore. The veins contain paragenetically later chalcocite ± euhedral pyrite, neodigenite, and djurleite. The late chalcocite encloses patches of earlier high chalcocite. The calcite stage is nearly barren and only accompanied by minor pyrite. The core of the veins locally contains late covellite and goethite; in places the vugs are filled with alunite and kaolinite that probably accompanied partial dissolution of calcite. Harmotome, a Ba-bearing zeolite, is a common mineral within the vugs as well as chalcedony. The veins also show evidence of widespread and polyphase cataclasis, marked by the presence of cataclasitic breccias.

Downwards, the veins grade into small fractures within the massive sulphides made up of pyrite and quartz. In contrast, upwards, the veins terminate in large breccia bodies that contain fragments of massive sulphides partially replaced copper sulphides and supported by vuggy calcite and euhedral djurleite, similar to those described by Melchiorre and Williams (2001) and Melchiorre and Enders (2003) in supergene zones of the Great Australia and Morenci deposits, respectively.

Postdating, the epithermal veins and breccia bodies are some delicate botryoidal aggregates of sulphides that fill open fractures, cement fault breccias, or coat individual djurleite-chalcocite crystals. These coatings include an early zone of galena covered by micrometer-thick delicate bands of chalcopyrite, bornite, chalcocite, enargite, and tennantite (Fig. 5o). Blake (2008) also described secondary veins composed of intergrown enargite and covellite that we have not observed.

Secondary alteration of host rocks

The siliciclastic and volcanic rocks beneath the Miocene paleosurface, adjacent to the faults and in the stockwork zone, show a major secondary alteration superimposed on the hydrothermal assemblages. The latter assemblage is replaced by an advanced argillic assemblage (Rye et al. 1992) that includes irregular but large zones enriched in kaolinite and alunite and variable amounts of quartz and montmorillonite (Fig. 5i) with abundant disseminated to semi-massive pyrite and local remnants of stockwork quartz veins. These altered zones host abundant, centimeter-thick veins of massive alunite (Fig. 5j).

This zone of advanced argillic alteration is interpreted as secondary and having formed during the downward percolation and reaction of the dacite with the acidic fluids formed during the subaerial oxidation of the massive sulphides; these percolating fluids likely lost all of their copper during formation of the overlying cementation zone. What is unusual at Las Cruces is that the alteration is spatially associated with pyrite and not with iron oxides or secondary copper minerals, as typically occurs in supergene environments.

Silica-rich rocks are widespread as large lenses within the gossan, the red and black rocks, and the host rocks beneath the unconformity. Quartz-rich zones, up to 15–30 m thick, are similar to the large secondary silica zones found elsewhere in the IPB (Velasco et al. 2013). These siliceous rocks are composed of massive to brecciated white quartz with accessory barite, anglesite, siderite, and pyrite as well as local gold and silver enrichments; in places, the porosity is infilled by galena. A correlation seems to exist between the abundance of quartz in the gossan and lateral distance from the massive sulphide (Knight 2000), with quartz locally forming a silica cap above or beneath the gossan that in places yields large zones of uncemented "quartz sands" that form large lensoidal bodies. The formation of this gossan-related quartz is likely related to remobilization of silica during oxidation of the massive sulphides. Morris and Fletcher (1987) reported that the solubility of silica increases during the oxidation of Fe^{2+} to Fe^{3+}; silica thus would be leached from the host volcanic rocks and precipitated in the gossan. Large zones of secondary quartz are common in secondary sulphide deposits, such as Flambeau, Wisconsin (May 1977), Zapadno-Ozernoe, Russia (Belogub et al. 2008), and Tambo Grande, Peru (Winter et al. 2004); this last deposit contains a 2-m-thick layer of Ag-rich sandy quartz that has been interpreted as having a bacteriogenic origin.

Adjacent to the F1 fault system is a major silicification zone that has affected all of the host rocks, developing a selvage of grey to black chert with disseminated pyrite, in places including stratabound zones of silicification that spread out from the faults. Locally, ghosts of bladed calcite are present. This second silicification event must be related to fluid circulation along the Alpine fault system.

Temperature of ore-forming processes

One of the most intriguing features of the Las Cruces deposit is widespread evidence that the formation of some of the secondary mineralization was related to the circulation of relatively hot fluids. The veins in the advanced cementation zone and the epithermal veins contain abundant early high chalcocite, indicating temperatures of precipitation in excess of 103 ± 3 °C (Roseboom 1966; Barton and Skinner 1979). The presence of hydrothermal breccias and of pseudomorphs or ghosts of bladed calcite in the silica replacements are indicative, at least locally, of boiling, which is consistent with the epithermal textures of the veins. The presence of bladed calcite is widely used as a criterion for boiling in hydrothermal systems (Simmons and Christenson 1994), because phase separation produces rapid fractionation of gasses, including CO_2, into the vapor phase and supersaturation in calcite. However, these relatively hot fluid events must have been intermittent, since djurleite and chalcocite, some of the most abundant sulphides, only are stable below 93 °C (Roseboom 1966; Potter 1977). The cavities within the breccia contain abundant harmotome, a Ba-zeolite typical of hydrothermal systems (Deer et al. 1966); the similar mineral phillipsite has a range of formational temperatures from ca. 60 to 80 °C (Chipera and Apps 2001).

The quartz and calcite in the veins and breccias host some fluid inclusions. These inclusions occur isolated within the crystals and are <5 to 20 μm in diameter. They have intermediate densities and locally rather high salinities of up to 9.1 wt% NaCl equiv. (Knight 2000); the highest values are significantly above those of present-day waters (<0.2 wt% NaCl equiv.; Table 2). The few fluid inclusions that homogenize to a liquid do so between 120 and 210 °C (Knight 2000); no low-density fluid inclusions have been found, but this could be due to very limited sample coverage or the low wetting effect of the aqueous vapor that favors quick upward migration.

As a whole, these data suggest that the advanced cementation zone and the epithermal veins formed at temperatures that were at times above 100 °C accompanied by episodic boiling. These abnormally high temperatures for a secondary zone could explain the abundance of unusual sulphides uncommon to supergene environments such as chalcopyrite, enargite, tetrahedrite-tennantite, and bornite.

No geothermometers exist for the formation of the biogenic zone. Measured present-day temperatures of the Niebla-Posadas aquifer (18–31 °C; Table 2) and the presence of current microbial activity (Tornos et al. 2014) suggest that temperatures of this zone never surpassed ca. 113 °C, the maximum permitted for the growth of sulphate-reducing bacteria (Stetter 1996). However, in the black rock, proustite coexists with its low-temperature

polymorph, xanthoconite. The available data (Roland 1970) indicate that proustite is only stable above 180–202 °C. This probably excessive temperature conflicts with the abundance of smythite that has an upper thermal limit near 53 °C (Furukawa and Barnes 1996), and the presence of other silver sulphides such as sternbergite and acanthite that have stability limits below 177 °C (Barton and Skinner 1979).

Methods

Representative samples from the different types of mineralization and host rocks have been analyzed for conventional stable and radiogenic isotopes. The analytical procedures are described below and results presented in Tables 3 and 4. Stable isotope measurements of goethite, carbonates, sulphides, and water were carried out at the Stable Isotope Laboratory of the Instituto Andaluz de Ciencias de la Tierra (CSIC-UGR) in Granada and the Centro de Astrobiología (Madrid). Carbon dioxide was obtained by reaction of the carbonates (McCrea 1959; Al-Aasm et al. 1990) and dissolved inorganic carbon (DIC; Salata et al. 2000) with 100 % phosphoric acid. Water was analyzed using the CO_2–H_2O equilibration method of Epstein and Mayeda (1953). Sulphur isotopes of aqueous sulphate, sulphates, and sulphides were measured by precipitation of $BaSO_4$ from solution, followed by combustion with V_2O_5 and O_2 at 1030 °C (Révész and Haiping 2007). Only the deuterium isotope composition of goethite is evaluated because the analyzed $\delta^{18}O$ values are unrealistic and probably reflect fine-grained mixtures of goethite, quartz, and hematite. The strontium isotope composition was obtained at the CAI Geocronología y Geoquímica Isotópica of the Universidad Complutense de Madrid, following the procedure described in Galindo et al. (1997). The $\delta^{18}O$ isotopic composition of quartz was obtained by fluorination at the Servicio General de Isótopos Estables of the University of Salamanca (http://nucleus.usal.es/isotopos/presentacion). Fractionation factors used for the calculations are from Zheng (1993) (quartz-H_2O), Friedman and O'Neil (1977) (calcite-H_2O and calcite/siderite-CO_2) and Carothers et al (1988) for siderite-H_2O.

Ar-Ar ages of alunite were determined by the Nevada Isotope Geochronology Laboratory (see http://geoscience.unlv.edu/nigl/equipment.html). Measured atmospheric $^{40}Ar/^{36}Ar$ ratios were 278.41 ± 0.44 % during this work, thus a discrimination correction of 1.0614 (4 AMU) was applied to the measured isotope ratios. Whole-rock analyses were performed at the Instituto Geológico y Minero de España (IGME) by XRF and ICP-MS methods following standard procedures (www.igme.es).

Geochemistry

Isotope geochemistry

The oxygen and deuterium isotope values of the Niebla-Posadas aquifer and the deep reservoir are indistinguishable at both mine and regional scales ($\delta^{18}O$ −5.8 to −3.9‰; δD −35 to −17‰; Table 2 and ESM Table 1; see also Scheiber et al. 2015). These values are within the range for regional rainfall as determined in the nearby station of Moron ($\delta^{18}O$ −9.1 to −0.1; δD −62 to 64‰; IAEA 2015), but show a significantly smaller variation, which suggests major isotopic homogenization during underground flow. All of these values are near the Global Meteoric Water Line indicating minor O–H isotopic exchange with the host rocks and absence of non-equilibrium evaporation (Fig. 6). The residual goethite has δD values (−111 to −60‰) between those of the groundwater and that of the water calculated for the gossan of the San Miguel mine using the fractionation equation of Yapp (1987), the latter characterized by very low δD values (−148 to −136‰; Alvaro 2010).

The carbon and strontium isotope compositions of the carbonates in the mineralization are also indistinguishable from those of the waters in the two reservoirs (ESM Table 1). Scheiber et al. (2015) interpreted the chemical differences between the Niebla-Posadas aquifer and the deep reservoir as recording a different chemical evolution of a parental rainwater that mixed with seawater trapped in pores, or to variable cation exchange with the host rocks. The sulphur, oxygen, and strontium isotope compositions of the biogenic zone and the epithermal veins (see below) are also consistent with mineral precipitation from water similar to that of the aquifer. The composition of the water(s) associated with the advanced cementation zone remains speculative.

The carbon and oxygen isotope compositions of the carbonates are shown in Table 3 and plotted in Fig. 7. Overall, the $\delta^{18}O$–$\delta^{13}C$ values of the carbonate of the secondary mineralization at Las Cruces are strikingly different from those of the earlier carbonate-rich hydrothermal alteration that is widespread in host rocks to the volcanogenic massive sulphide deposits of the IPB (Tornos et al. 1998) that have more negative $\delta^{18}O$ and more positive $\delta^{13}C$ values.

Carbonates of the epithermal veins and the biogenic zone have broadly similar oxygen ($\delta^{18}O$ +24.9 to +27.9‰) and strontium ($^{87}Sr/^{86}Sr$ 0.7101–0.7104) isotope values but the black and red rocks have more negative $\delta^{13}C$ values (−37 to –20‰ and –42 to −18‰, respectively) than calcite in the veins (−30 to –12‰). Furthermore, the $^{87}Sr/^{86}Sr$ values of the carbonates in the mineralization closely match the isotope composition of the presently flowing water ($^{87}Sr/^{86}Sr$ 0.7102–0.7104; Fig. 8, Table 3 and ESM Table 1). The $\delta^{18}O$ composition of the calcite is consistent with its precipitation from the flowing water at temperatures below 46 °C, in agreement with

Table 3 Stable (C–O–H–S) and radiogenic (Sr) isotopic compositions of whole rocks and minerals from secondary alteration zone

Sample	Description	Mineral	$\delta^{18}O_{SMOW}$ ‰	δD_{SMOW} ‰	$\delta^{13}C_{PDB}$ ‰	$^{87}Sr/^{86}Sr$	Error ($\times 10^{-6}$)
LCM-182	Arcilla de Gibraleon Fm. Whole rock marl	WR				0.709330	5
LCM-183	Arcilla de Gibraleon Fm. Whole rock marl	WR				0.709091	6
LCM-184	Arcilla de Gibraleon Fm. Whole rock marl	WR				0.709064	5
LCM-171	Basal Tertiary Sandstone	WR				0.709080	4
LCM-190	Basal Tertiary Sandstone	WR				0.710175	6
LCM-191	Basal Tertiary Sandstone	WR				0.710278	4
LCM-013	Residual gossan	goe (hm-Q)	10.7	−78		0.710159	5
LCM-016	Residual gossan	goe (hm-Q)	15.9	−68			
LCM-035	Residual gossan	goe (hm-Q)	9.3	−75			
LCM-165	Residual gossan replaced by red rock	goe (hm-Q)	6.8	−102			
LCM-166	Residual gossan replaced by red rock	goe (hm-Q)	9.7	−111			
LCM-036	red rock	sid				0.710199	6
LCM-029	red rock	sid				0.710361	9
LCM-048 F	red rock	sid				0.710083	9
LCM-164	red rock	sid				0.710363	6
LCM-174	red rock. Euhedral siderite crystals	sid				0.710353	5
LCM-042	Residual gossan replaced by black rock	goe (hm-Q-cc)	6.9	−70			
LCM-063	Residual gossan replaced by black rock	goe (hm-Q-cc)	2.4	−78			
LCM-229	Residual gossan replaced by black rock	goe (hm-Q-cc)	3.2	−60			
LCM-022	black rock	cc				0.710254	8
LCM-045	black rock	cc				0.710286	9
LCM-41B	black rock	WR				0.710095	5
LCM-033	Silicified felsic volcanic rock	WR				0.710252	9
LCM-399	Silica-rich alteration: goethite intergown with quartz	goe (hm-Q)	10.4	−89			
LCM-399	Silica-rich alteration with siderite	sid	24.2		−31.3		
LCM-077'A	Hydrothermal breccia	cc	26.1		−25.2	0.710271	5
LCM-087	Hydrothermal breccia	cc	27.9		−24.2	0.710430	5
LCM-095	Hydrothermal breccia	cc	24.2		−15.5	0.710266	5
LCM-123	Hydrothermal breccia	cc	27.2		−21.9		
LCM-217	Hydrothermal breccia	cc	23.5		−23.3		
LCM-075	Epithermal vein: calcite + quartz	cc	23.0		−14.4	0.710389	5
LCM-120	Epithermal vein: calcite + quartz	cc	25.0		−11.8	0.710244	5
LCM-121	Epithermal vein: calcite + quartz	cc	22.5		−13.8	0.710199	4
LCM-123	Epithermal vein: calcite + quartz	cc	27.4		−29.6	0.710247	5
LCM-147	Epithermal vein: calcite + quartz	cc	27.8		−24.4		
LCM-402	Epithermal vein: calcite + quartz	cc	26.1		−30.9		
LCM-403	Epithermal vein: calcite + quartz	cc	26.3		−30.6		
LCM-404	Epithermal vein: calcite + quartz	cc	24.5		−26.0		
LCM-405	Epithermal vein: calcite + quartz	cc	23.0		−23.3		
LCM-409	Epithermal vein: calcite + quartz	cc	22.1		−21.9		
LCT-49	Epithermal vein. Quartz	Q	12.8				
LCT-51	Epithermal vein. Quartz	Q	12.5				
CLC-SK1	Epithermal vein. Quartz	Q	14.3				
LCT-13a	Epithermal vein. Late chalcedony	Q	26.5				
LCT-13b	Epithermal vein. Late chalcedony	Q	26.8				
LCT-98	Acid alteration	Alunite				0.710413	2
LCT-99	Acid alteration	Alunite				0.711158	2
LCT-028	black rock. Late vein	sid	21.5		−19.0	0.710378	5
LCM-204	Late Veinlets of calcite in massive sulphides	cc	23.2		−16.7		

Analysis of δ^{18} O in quartz at Servicio General de Isótopos Estables of the University of Salamanca; other stable isotopes at Stable Isotope Laboratory of the Instituto Andaluz de Ciencias de la Tierra. Analytical error better than ±0.1 ‰ (O, C), ±1 ‰ (D). Sr isotopes analyzed at CAI Geocronología y Geoquímica Isotópica of the Universidad Complutense de Madrid

cc calcite, *goe* goethite, *hm* hematite, *Q* quartz, *sid* siderite, *WR* whole rock

the estimated temperatures within the aquifer and those during formation of the biogenic zone, thus indicating that $\delta^{18}O$ values of the carbonates are buffered by water in the aquifer. The estimated temperatures are significantly lower than those of quartz precipitation in the epithermal veins using the $\delta^{18}O$ values of the water in the aquifer and the fractionation factor of Zheng (1993). Our preferred interpretation is that oxygen in the calcite has equilibrated with late fluids circulating through the vein, or the calcite infillings are late with respect to the quartz and barite. Textural relationships support this late paragenetic hypothesis. The carbonates have systematically lower $\delta^{13}C$ values than the associated water (see ESM Table 1), defining a clear mixing line between fluids with high and low $\delta^{13}C$ values while maintaining constant $\delta^{18}O$ values.

Table 4 Sulphur isotope data for sulphides

Sample	Type	Mineral	$\delta^{34}S$ ‰
LCM-042-1	Advanced Cementation Zone—massive chalcocite	cc	21.5
LCM-042-2	Advanced Cementation Zone—massive chalcocite	cc	21.5
LCM-090	Advanced Cementation Zone—chalcocite cementing pyrite	cc	7.5
LCM-091	Advanced Cementation Zone—chalcocite cementing pyrite	cc	6.1
LCM-094	Advanced Cementation Zone—chalcocite veins in massive sulphides	py	16.0
LCM-204	Advanced Cementation Zone—chalcocite veins in massive sulphides	cc	7.8
LCT-048	Advanced Cementation Zone—massive chalcocite vein	cc	9.9
LCT-082-2	Advanced Cementation Zone—massive chalcocite vein	cc	11.7
LCT-084-1	Advanced Cementation Zone—massive chalcocite vein	cc	16.3
LCT-084-2	Advanced Cementation Zone—massive chalcocite vein	cc	16.3
LCT-085-1	Advanced Cementation Zone—massive chalcocite vein	cc	16.4
LCT-085-2	Advanced Cementation Zone—massive chalcocite vein	cc	17.3
LCT-085-3	Advanced Cementation Zone—massive chalcocite vein	cc	12.0
LCT-086-1	Advanced Cementation Zone—massive chalcocite vein	cc	8.1
LCT-021	Cementation Zone—veinlets of chalcocite in massive sulphides	cc + py	9.3
LCT-023	Cementation Zone—replacement of massive sulphides by chalcocite	cc + py	7.1
LCT-029	Cementation Zone—chalcocite coating massive sulphides	cc	6.3
LCT-052	Cementation Zone—chalcocite coating massive sulphides	cc	8.8
LCT-060	Cementation Zone Cementation Zone—chalcocite coating massive sulphides	cc	5.8
LCM-087	Epithermal vein	py	1.6
LCM-091	Epithermal vein	py	5.3
LCM-092	Epithermal veins	cc	13.3
LCM-095	Epithermal vein	py	5.9
LCM-123	Epithermal vein	py	8.4
LCM-147	Epithermal vein	cc	-0.5
LCM-217	Epithermal vein	cc	7.1
LCM-409	Epithermal vein	cc	5.9
LCM-410	Epithermal vein	cc	2.1
LCT-033	Epithermal veins	cc	4.8
LCT-063	Epithermal vein	cc	15.3
LCM-274-1-1	HC4 ore	cv	17.5
LCM-274-1-2	HC4 ore	cv	17.6
LCM-274-1-3	HC4 ore	cv	11.4
LCM-274-1-4	HC4 ore	cv	16.51
LCM-274-2-1	HC4 ore	cv	11.3
LCM-274-2-2	HC4 ore	cv	15.8
LCM-274-2-3	HC4 ore	cv	16.3
LCM-274-3-1	HC4 ore	cv	13.4
LCM-274-3-2	HC4 ore	cv	11.0
LCM-274-3-3	HC4 ore	cv	13.3
LCT-026	HC4 ore—veins covellite	cv	5.4
LCT-036a	HC4 ore—covellite replacing sphalerite	cc	7.7
LCM-003	Massive sulphides	wr	1.1
LCM-093	Massive sulphides	py	9.5
LCM-008	Sandy Barren Pyrite	py	0.3
LCM-086	Sandy Barren Pyrite	py + (gn)	4.8
LCM-066	Sandy Barren Pyrite	py	1.9
LCM-124	Sandy Barren Pyrite	py	6.4
LCM-142	Sandy Barren Pyrite	py	4.9

Analysis vs CDT. Analytical precision better than ±0.2‰

cc chalcocite, *cv* covellite, *gn* galena, *py* pyrite, *wr* massive sulphide whole rock

The $\delta^{18}O$ values of quartz in the epithermal veins determined in this study (+10.1 to +12.8‰) are similar to those of +11.5 to +14.7‰ reported by Knight (2000). Equilibration temperatures ($\Delta_{quartz\text{-}H2O}$) with water in the aquifers are between 107 and 162 °C (avg. 125 °C), consistent with results from the aforementioned independent geothermometers. The late chalcedony infilling cavities have much higher $\delta^{18}O$ values (+26.5 to +26.8‰) that are consistent with precipitation at low temperatures (34–40 °C) from circulating groundwater.

The Sr isotope ratios of the carbonates within the secondary mineralization (Table 3) display a relatively narrow range from 0.7101 to 0.7104; these values are strikingly similar to those of the presently inflowing water, and support the premise that the biogenic zone and the epithermal veins formed in equilibrium with fluids isotopically similar to those flowing

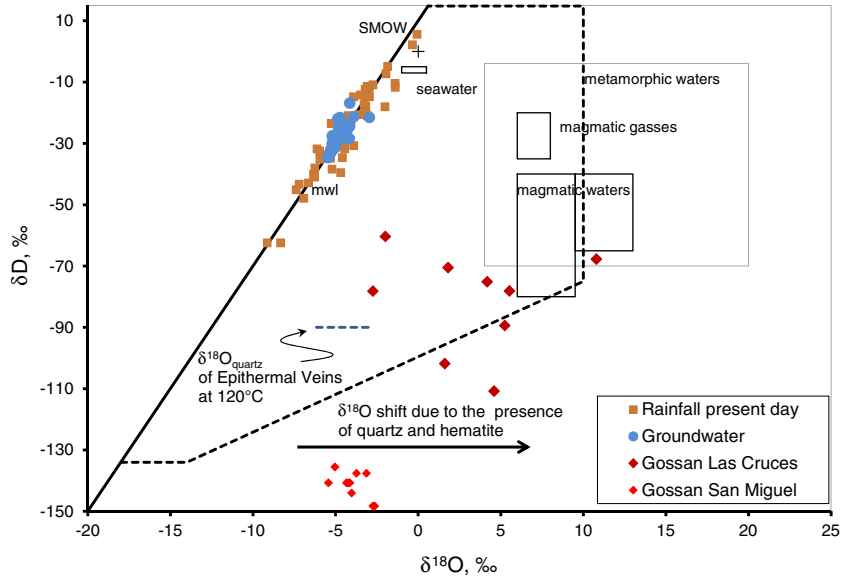

Fig. 6 $\delta^{18}O$-δD diagram showing isotopic compositions of groundwater and of secondary alteration zone at Las Cruces using the $\Delta^{18}O_{goethite\text{-}water}$ and $\Delta D_{goethite\text{-}water}$ fractionations of Yapp (1987; 2007), respectively. Calculated $\delta^{18}O_{fluid}$ values of goethite at Las Cruces and San Miguel are shifted to high values due to variable amounts of included quartz and hematite. Isotopic composition of water in equilibrium with quartz from the epithermal veins (only $\delta^{18}O$ data) has been calculated for average temperature of 120 °C using $\Delta^{18}O_{quartz\text{-}H2O}$ fractionation of Turpin et al. (1990). Fields for isotopic compositions of different types of waters are from Sheppard (1986)

today through the aquifers. These Sr isotope ratios are more radiogenic than those of the mafic rocks (0.7037–0.7067) and far less radiogenic than the present-day $^{87}Sr/^{86}Sr$ values of the PQ Group (0.7324–0.7748) in the IPB (Tornos 2006); significantly, they match the lower part of the range of values for the felsic volcanic rocks (07083–0.7850). Together, the combined Sr-C-O data show that all of the analyzed samples are isotopically different from the Tertiary marl that has low $^{87}Sr/^{86}Sr$ values (<0.7093) and high $\delta^{18}O$ and $\delta^{13}C$ values (30.8–33.6‰ and −1.8 to −0.8‰, respectively; Tornos et al. 2014), likely inherited from Messinian seawater that had $^{87}Sr/^{86}Sr$ ratios near 0.7086–07092 (Roveri et al. 2014). The sandstone hosting the aquifer shows both low and high Sr isotope values (0.70908 and 071018–0.71028), suggesting that these data represent a mixture of water inherited from the basement and the inflowing water.

A large database exists for $\delta^{34}S$ values from Las Cruces with more than 200 determinations that cover all styles of mineralization (Knight 2000; see also Table 4). In detail, there are significant differences among the types of mineralization. The $\delta^{34}S$ values of the massive sulphides (−6.8 to +10.3‰) are near the highest values of the shale-hosted deposits in the southern IPB that overall range from −33.2 to +18.2‰; (Velasco et al. 1998; Tornos 2006), and well above those of the adjacent Aznalcóllar-Los Frailes VMS deposits (−8.1 to +5.6‰; Velasco et al. 1998). As is typical in the Southern

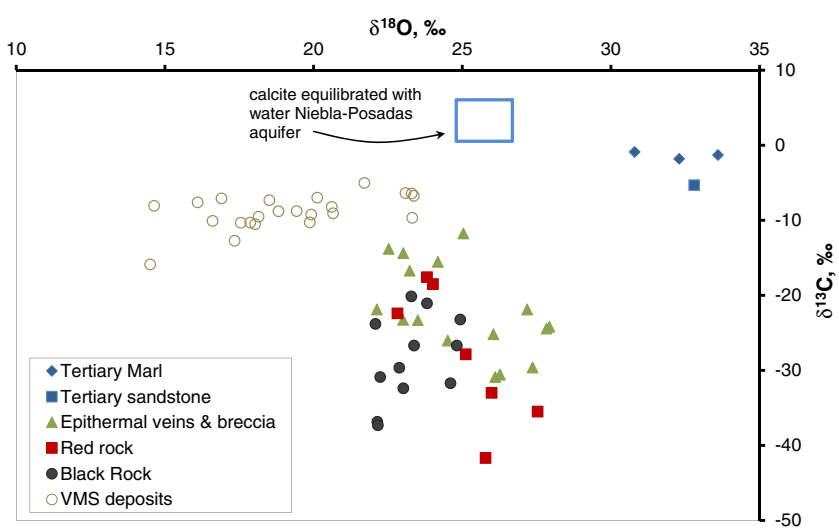

Fig. 7 Carbon-oxygen isotope composition of carbonates from biogenic zone and epithermal veins and breccias, compared with those from overlying Tertiary sediments, calcite equilibrated with the Niebla-Posadas aquifer, and hydrothermal carbonate from the IPB. Modified from Tornos et al. (2014)

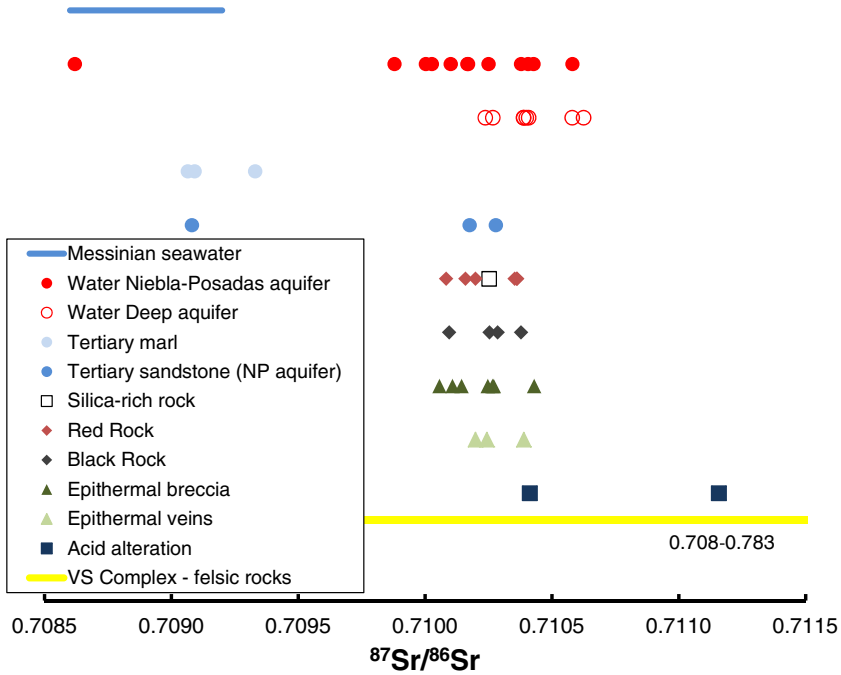

Fig. 8 Variation of Sr isotope compositions of rocks and reservoirs at Las Cruces and surrounding region

IPB, sulphur isotope compositions of the massive sulphides display more negative values than the associated stockwork sulphides (+2 to +16.4‰).

The $\delta^{34}S$ values of sulphides in the biogenic zone are significantly higher (mostly +19 to +24‰) than those of the underlying massive sulphides and the cementation zone rocks (Fig. 9). These values are also more enriched in ^{34}S than the sulphate in the water currently flowing through the Niebla-Posadas aquifer, which has a large range of values, between −17 and +22 per mil (ESM Table 1; Scheiber et al. 2015). This water is SO_4-rich (16–42 μg/g); the origin of elevated aqueous sulphate having such variable $\delta^{34}S$ values is unknown. The trend is, however, compatible with mixing of the Niebla-Posadas water—derived from atmospheric sulphate and oxidized sulphides in the basement rocks—with seawater sulphate of Miocene to present times ($\delta^{34}S \approx 22$‰; $\delta^{18}O \approx 14$‰; Claypool et al. 1980; Paytan et al. 1998). This model suggests that recharged rainwater could have gradually mixed with trapped seawater in sedimentary rocks and the basement. Alternatively, Manzano et al. (2004) proposed that it comes from rainwater contaminated with sulphate derived from local fertilizers. Scheiber et al. (2015) interpreted the observed coupled $\delta^{18}O$–$\delta^{34}S$ evolution, from low to high values at the aquifer scale, as reflecting gradual biogenic sulphate reduction during evolution from the recharge zone to the mine site, a model that agrees with the observed gradual depletion in aqueous $SO_4^{=}$ accompanied by an increase in H_2S. These data nevertheless leave doubt that some sulphate reduction took place in the aquifer before interacting with the orebody.

Regardless of the origin of this ^{34}S-enriched sulphate in the aquifer, the $\delta^{34}S$ signature of the biogenic zone indicates that the contained sulphides precipitated from this late aqueous sulphate with only minor isotope fractionation. Excluding TSR processes, which are unlikely to take place at these low temperatures below 150 °C (Machel 2001), the sulphate reduction must be relate to anaerobic metabolism of microorganisms (BSR).

The remaining secondary mineralization, including the cementation zone (−2.4 to +21.2‰), the advanced cementation zone (+6.1 to +21.7‰), the HC4 ore (+5.4 to +17.6‰), and the epithermal veins and breccias (−0.5 to +13.3‰) have $\delta^{34}S$ values that partially match those of the massive sulphides but are also shifted to more positive values of up to +22 per mil (Fig. 9). Such a trend cannot be attributed to isotope fractionation due to oxidation, nor to cooling, and probably represents the mixing of inherited sulphur from the hosting massive sulphides with a different and isotopically heavier source; in this context, the most likely derivation is also via BSR but with minor isotope fractionation. The sandy barren pyrite has $\delta^{34}S$ values between +0.3 and +6.4 per mil that could be inherited from the massive sulphides.

Ar-Ar dating

Five alunite samples were selected for Ar-Ar dating. Three samples (S427M14, S427104, and S427.85) are of disseminated alunite from acid-altered volcanic rocks located below the red rock. Three others (S43325m, S43325-1, and S433.256) are from massive alunite infilling veins. The results are shown in ESM Table 3 and Fig. 10.

The alunite veins show consistent plateau ages (10.2 ± 0.2 to 11.17 ± 0.2 Ma) and inverse isochron ages (10.84 ± 0.07 to

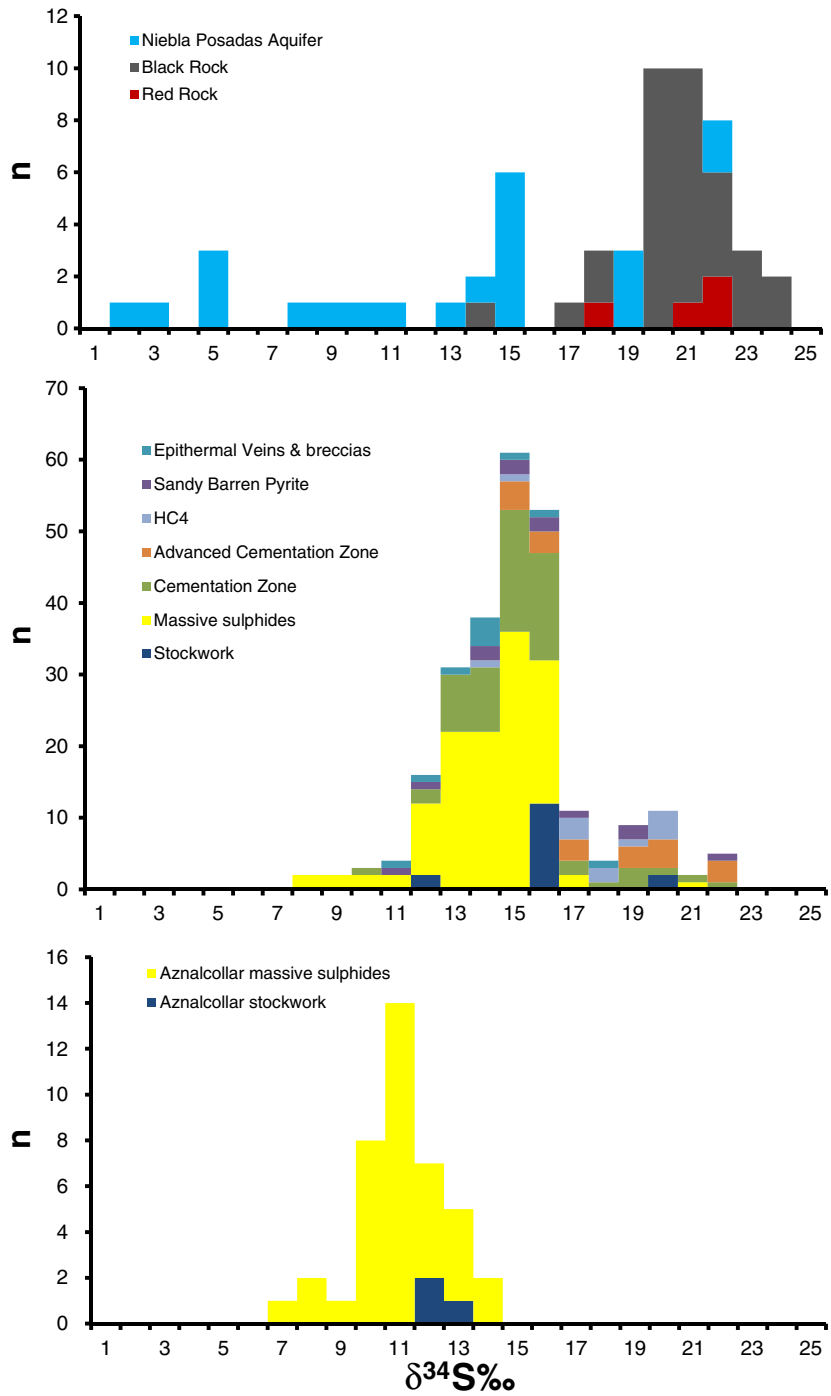

Fig. 9 Sulphur isotope geochemistry of mineralization and groundwater at Las Cruces. Diagram includes data of Knight (2000), Tornos et al. (2014) and references listed in Table 4

11.19 ± 0.23 Ma) (Fig. 10). If isochron ages are considered the most reliable, then the major mineralizing event took place in less than 0.7 m.y. during the Tortonian. This age is significantly older than that of the supergene alunite in the San Miguel deposit that has plateau ages of 7.30 ± 0.25 and 7.77 ± 4.02 Ma (Velasco et al. 2013) or the Tharsis deposit (7.52 ± 0.3 and 5.53 ± 0.14 Ma; Capitán 2006). Jarosite from the lowermost supergene profile at San Miguel has Ar-Ar plateau ages of 3.54 ± 0.16 and 0.86 ± 0.02 Ma (Velasco et al. 2013). Thus, the age of acid alteration at Las Cruces is the oldest among the recorded supergene ages in the IPB, and probably represents a "frozen" age because the gossan/cementation/acid alteration system there ended during burial below the marls, whereas in the other deposits, these systems continued maturing until present times.

Two samples of the felsic rocks that display acid alteration (S427M14 and S527.104) lack of plateau or inverse isochron ages. If the cause of these discordant age spectra is excess

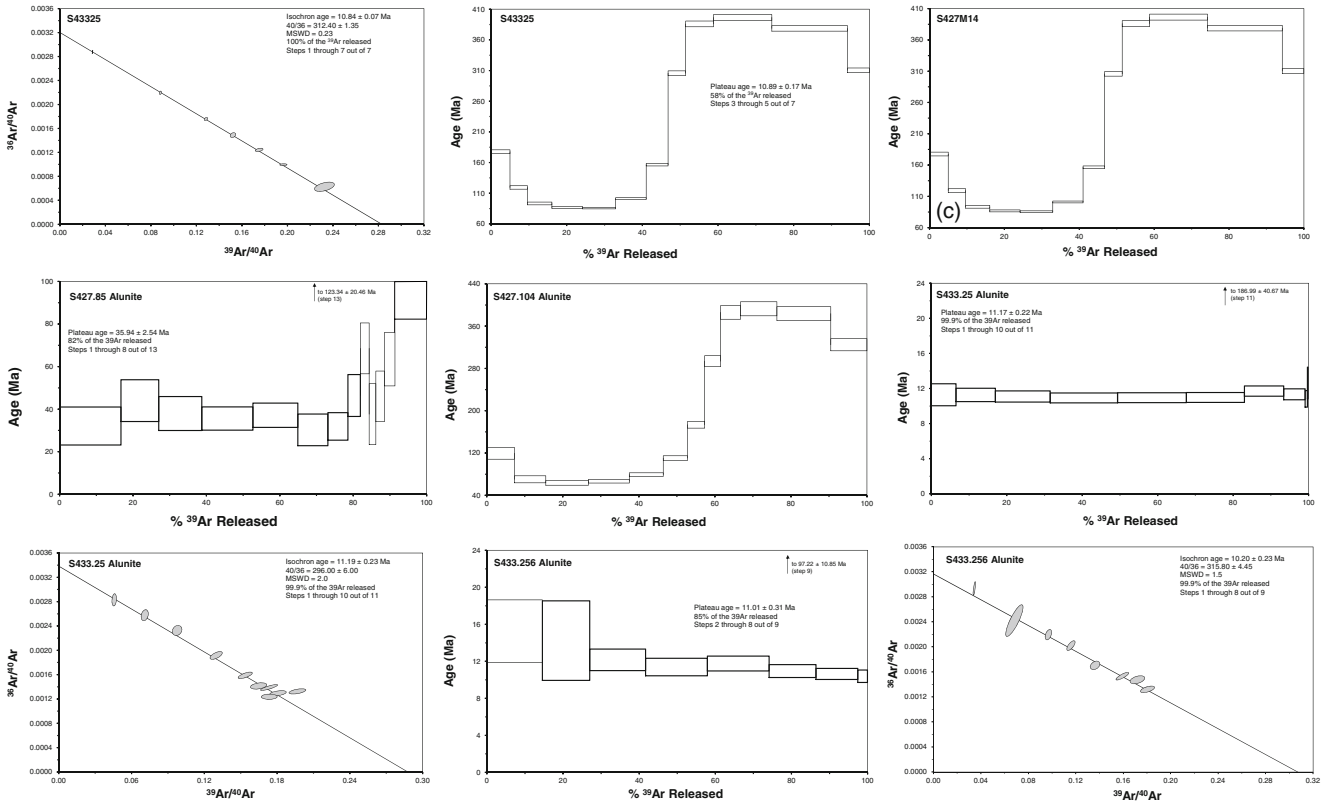

Fig. 10 Plateau and isochron ^{40}Ar–^{39}Ar ages of rocks from advanced argillic alteration zone at Las Cruces

argon, then the most conservative interpretation is that the youngest age of the age spectrum (≈85.6 and ≈63.5 Ma) is the most reliable. The total gas ages (249.5 ± 0.6 and 206 ± 1.7 Ma, respectively) probably do not have any geological meaning because during that time the orebody was buried. Sample S427.85 has a plateau age of 35.9 ± 2.5 Ma, which is close to the total gas age (45.5 ± 2.4 Ma). Although these ages are consistent with subaerial exposure of the massive sulphides and could thus reflect early formation of the secondary zones, they also may reflect mixing of Ar from different events, including massive sulphide formation, Variscan deformation, and secondary alteration.

Discussion: superimposed ore-forming events

Las Cruces differs from other secondary deposits worldwide and other outcropping VMS deposits of the IPB by having the following: (a) a large, high-grade, structurally controlled, high-temperature (>100 °C?) cementation zone with unusual supergene minerals such as high chalcocite, enargite, pyrite, bornite, and chalcopyrite that occur as open-space fillings and postdate the classical, low-grade cementation zone; (b) an "epithermal event"; and (c) red and black rocks that formed by replacing a gossan beneath Tertiary marls.

Individual events at Las Cruces are characterized by major changes in physicochemical conditions and separated from the other events by abrupt geochemical changes. Mineral assemblages shown in Table 1 apparently formed in rather isolated sub-systems inherited from the pre-Late Tortonian, subaerial supergene system. The cementation zones are enriched in Cu–(As–Sb), whereas the biogenic zone has high contents of Pb, Ba, As, Sb, Hg, Ag, and Au. Although the primary sulphide assemblage is rich in Zn, no Zn-rich minerals are known in the secondary assemblage, and hence, all of the Zn is interpreted as having been leached away.

Most previous studies have recognized the polyphase nature of the Las Cruces deposit but different workers disagree on the relative importance of each event. The majority agree that the cementation zone formed under subaerial conditions and that the capping red and black rocks record the replacement of a former gossan beneath the marl cap (Blake 2008; Yesares et al. 2011b; 2014; 2015; Tornos et al. 2012a). As noted above, our interpretation is that the distinctive features of Las Cruces reflect a specific tectonic and hydrologic evolution directly related to the evolution of the local hosting Tertiary basin that is not present in the other deposits.

To our knowledge, there is no other deposit similar to Las Cruces, except perhaps the small mineralization at Zapadno-Ozernoe in the Urals. Here, Belogub et al. (2003; 2008) have described galena-rich secondary assemblages in a complex secondary profile that includes residual pyrite sands and a silica-barite-rich layer separating the leached and oxidized zones.

The classic secondary deposit

We propose that the original paired gossan/cementation zone formed between exhumation of the massive sulphides at an unknown post-Variscan age and burial in late Tortonian times (ca. 7–8 Ma). As in other supergene systems of the IPB and elsewhere, subaerial exposure included erosion and weathering of massive sulphides accompanied by the formation of two separated domains, which are interpreted as the water-undersaturated oxidizing zone (gossan) and the saturated reduced zone. The latter is separated by the water table, as has been predicted by classical models of supergene alteration, involving the leaching of copper and zinc during the biogenic destruction of pyrite (Anderson 1982; Brimhall et al. 1985; Alpers and Brimhall 1989). Copper precipitates from oxidized descending water, where it reaches the phreatic zone that is more reducing and poor in free oxygen. The evolution of these systems is controlled by fluctuations in the water table and relationships with faults. Sato (1960) and Ague and Brimhall (1989) have shown that the commonly zoned assemblages found in cementation zones of secondary deposits are controlled mainly by changes in redox state. In contrast to the well-studied cementation zones in porphyry systems, those developed on VMS deposits have exceedingly low Cu/Fe ratios and almost no acid consumers, such that most of the secondary copper sulphides precipitate by cation exchange with other sulphides (Putnis 2009). The similarity of sulphur isotope values for the massive sulphides and the cementation zone is consistent with this mechanism, in which the sulphur of the neoformed sulphides is inherited from the precursor sulphides. Only in the unaltered host rocks and the stockwork zone do the secondary sulphides precipitate by changes in pH due to reaction of the fluids with minerals like feldspar or chlorite.

Onset of Alpine extension: the advanced cementation zone

The direct relationship between the advanced cementation zone and HC4 high-grade zones with the Alpine faults shows that basin compartmentalization during the formation of the Guadalquivir forearc basin was responsible of major ore upgrading. Close spatial association of these high-grade ore zones with the F1 fault suggests formation related to fluid overpressure that hydraulically fractured the hosting massive sulphides and localized the secondary copper mineralization.

The occurrence of a significant part of the chalcocite as open-space fillings within the massive veins records precipitation directly from the fluid. Leaching of reduced sulphur from the host massive sulphides would imply their dissolution beneath the water table under reducing conditions—the environment that favors their precipitation but not dissolution.

Mineralogically, the difference between the cementation zone at Las Cruces and other secondary copper deposits is the presence in the former of abundant pyrite, bornite, chalcopyrite, enargite, and tennantite. The evolution recorded in the veins and—to a lesser extent in the replacement ore—reflects a marked increase in sulphidizing conditions, from the pyrite-chalcopyrite assemblage to different types of chalcocite and covellite. Occurrence of delicate botryoidal textures in the cementation zone indicates local supersaturation, whereas the presence of coarse-grained chalcocite is more consistent with slow growth. During this evolution, the HC4 zone probably represented the lowermost part of the system where fluid mixing took place along the major fault that defines the footwall of the massive sulphides (Fig. 3). In this setting, perhaps the only mechanism able to form these veins is the mixing of descending acidic oxidized waters rich in sulphate and copper, with deep overpressurized and hot reduced fluids that ascended along the fault zone.

Calculations show the solubility of copper in a reduced and alkaline fluid is very low at temperatures below 120 °C (ca. $<10^{-10}$ μg/g); hence, it is unlikely that copper could be significantly mobilized by upwelling fluids within the vadose zone. Thus, we hypothesize that copper was transported with aqueous sulphate from the oxidizing cap of the deposit and precipitated where the fluid mixed with deep fluids rich in reduced aqueous sulphur. Mixing between an acidic and oxidized fluid and an alkaline and reduced one should promote the formation of a secondary sulphide assemblage, and the zonation observed in the veins in which early chalcopyrite is followed by bornite and chalcocite. Calculations also suggest that enargite becomes the stable copper phase at low to intermediate pH when As is present; if not, covellite is the predominant phase (Fig. 12a).

The higher $\delta^{34}S$ values of the cementation zone regarding the primary massive sulphides (Fig. 9) support the hypothesis that not all the sulphur is inherited from the protolith and some of it could derived from biologically mediated reduction of downward percolating sulphate with only minor isotope fractionation, in a manner similar to that proposed for the overlying biogenic zone (see below).

Related advanced argillic alteration formed by the reaction of the acidic and oxidized descending waters with the volcanic rocks affected by chlorite-quartz-pyrite alteration, a reaction that consumes much of the H^+. The overlying massive sulphides have little capability of buffering the pH, but were able to precipitate all of the available copper; the lack of Cu-bearing minerals in the advanced argillic zone indicates that the copper content of the descending fluids here was negligible. Coexistence of primary pyrite with the neoformed sulphates likely indicates widespread sulphate-sulphide chemical disequilibrium during the supergene alteration. These supergene acidic fluids were probably also responsible for major remobilization of the silica deposited near the major faults.

Our preferred interpretation for the formation of the advanced cementation zone at ca. 11.2 ± 0.2 to 10.8 ± 0.1 Ma is

that during the Tortonian (ca. 12–7 Ma), there were optimal conditions for the accelerated subaerial supergene alteration of the massive sulphides. This alteration probably took place in a rather tropical climate—warm with high rainfall (Sáenz de Galdeano and Vera 1992)—thus creating ideal conditions for the formation of a deep weathering profile. This process was synchronous with the extensional faulting that configured the Guadalquivir Basin, lowering the water table—perhaps due to a rift shoulder effect—and accelerating the process. In our interpretation, the sandy barren pyrite zone represents a zone of intense leaching in which the quick drop of the water table produced adeepening of the cementation zone but was unable to lower the basal level of the gossan at the same rate. This second event of cementation was superimposed on the earlier one.

At some stage, perhaps during the Late Tortonian, the basin was below seawater level and the massive sulphides interacted with seawater until they were covered and isolated by newly deposited clastic sediments and the overlying marl. This process potentially could have altered the mineralization and formed a submarine gossan, but in our study we have not found any geochemical evidence of such an event.

Hypothetically, the supergene system was quickly covered by the sediments of the basal transgressive Miocene, thus inhibiting interaction with seawater. Yesares et al. (2015) proposed that formation of the kaolinite and smectite as well as the high $\delta^{34}S$ values of the sulphides is related to this event, but it is unlikely that acidic alteration and sulphide precipitation took place in such a seawater-saturated environment; furthermore, we have not found any isotopic evidence of the involvement of seawater in the mineralizing process.

For Las Cruces, mass-balance calculations suggest that the size of the present-day gossan and products of its replacement (red and black rocks) are much smaller than those of the cementation zone, thus suggesting that most of the gossan was eroded. The minimum amount of eroded massive sulphides can be roughly estimated by the Cu content of the secondary zone. Formation of a cementation zone containing 16 Mt with 6.9 % of leachable Cu, derived from primary massive sulphides having on average 1.05 % Cu, indicates that the original mineralization was at least 140 Mt and that about the 75 % of the original orebody has been eroded. These figures, however, are probably maximum values because some of the copper was probably leached below the water table.

The epithermal event

The structure and mineralogy of the epithermal veins indicate formation due to episodic hydrothermal activity. This activity occurred during the development of widespread crack and seal textures, by quick cooling of a hot, silica-saturated, Ba-bearing fluid synchronously with mixing with a descending, cooler, and oxidized fluid. Isotopic similarities between the calcite in the veins and that in the biogenic zone suggest a similar origin (Figs. 7 and 8). The mineral assemblage including carbonates, barite, and quartz indicates neutral to alkaline fluid conditions and, as discussed above, at least intermittent boiling, which also favored the precipitation of calcite. However, the presence of calcite and barite cannot be explained by simple cooling or its reaction with the massive sulphides. The Sr and C–O isotope geochemistry is consistent with the veins being formed by mixing of waters similar to those currently flowing through the current deep reservoir and Niebla-Posadas aquifer, but at higher temperatures (107–143 °C). The sulphur isotope values additionally suggest that sulphide minerals within these veins inherited sulphur from the host cementation zone or the primary massive sulphides, but with only minor isotope fractionation occurring during sulphide precipitation.

The crosscutting relationships indicate that the epithermal veins postdate burial are of post-Tortonian age and probably are synchronous with formation of the biogenic zone. These veins are attributed to a waning epithermal system controlled by the Alpine faults, where the deep fluids—probably the hotter equivalents of the present-day deep reservoir—mixed with descending waters similar to those of the Niebla-Posadas aquifer.

The "epithermal" environment

One of the intriguing aspects of the Las Cruces deposit is the presence of zoned quartz-barite-calcite veins with epithermal features and the relative abundance of enargite, tennantite, and bornite within the secondary assemblage. Enargite is a fairly common secondary phase at Las Cruces (Knight 2000; Blake 2008; Yesares et al. 2015). It is mainly found associated with chalcocite of the advanced cementation zone or with chalcopyrite and bornite in the epithermal veins; as an accessory phase, it is intergrown with chalcocite in the cementation zone. Detailed EPMA analyses of the largest grains of enargite, typically intergrown with fine-grained chalcocite and replaced by tennantite, show a mixing trend among the three minerals (Fig. 11 and ESM Table 4). Blake (2008) described grains of enargite having close to stoichiometric compositions.

Enargite was regarded as primary by Blake (2008) but in this study, we have not found any evidence to support this interpretation. Within the IPB, enargite has been only reported as an accessory mineral in the primary ore at Neves Corvo (Gaspar 2002). Although some workers have described enargite as being characteristic of high-sulphidation epithermal systems (Hedenquist et al. 1993; Arribas 1995; Baumgartner et al. 2008; Bendezú and Fontboté 2009; Reed et al. 2013), this assumption seems not to be straightforward because enargite also has been found in very different ore-forming environments including Mississippi Valley-type

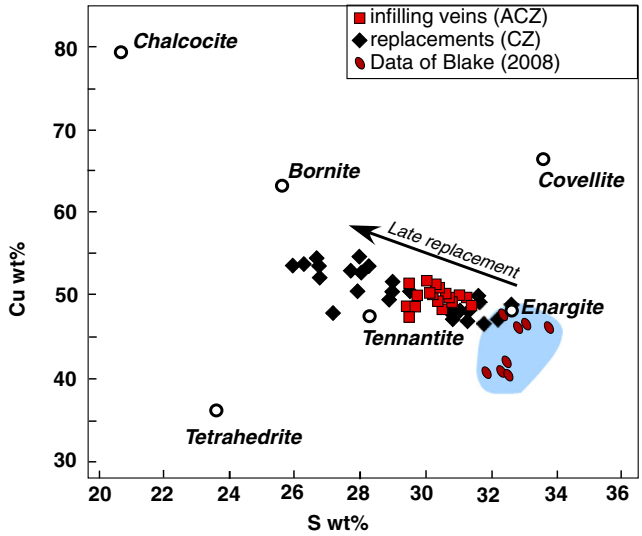

Fig. 11 EPMA analyses of enargite, including data from Blake (2008). *Open circles* represent stoichiometric compositions of most significant sulphides (*labelled*). *ACZ*, Advanced Cementation Zone; *ZC*: Cementation Zone

deposits (Heyl 1964; Leach et al. 1995), stratabound copper deposits (Sood et al. 1986), manto-like deposits (Kojima et al. 2009), VMS deposits (Scott et al. 2001), Tsumeb-like deposits (Melcher et al. 2006), and in zones of supergene alteration (Foley and Flohr 1998; Leverett et al. 2005).

There are few data available on the stability field of enargite. At high fS_2, it is stable at temperatures up to the sulphur condensation curve, and at low fS_2, it breaks down into tennantite + S_2. Occurrence of enargite in low-temperature deposits suggests that it is stable down to ambient temperatures; the upper thermal is close to 671 ± 1 °C (Barton and Skinner 1979). Figure 12a shows that at 50 °C and under highly reducing conditions, enargite can precipitate from a fluid having an As/Cu ratio similar to that of the water of the deep reservoir at Las Cruces, but only at pH below ca. ≈ 6.5. The stability field expands at lower pH. In systems low in As, the stable minerals are chalcopyrite, bornite, chalcocite, and covellite, whereas at high aAs^{3+}, these minerals are replaced by tennantite-enargite. The presence of high As contents can only be due to the involvement of relatively alkaline fluids in the formation of the cementation zone and epithermal veins (see below). Overall, these data show that the enargite-rich assemblages at Las Cruces are not the product of a high-sulphidation system, but more likely relate to low-temperature, secondary replacement processes in which the sulphide assemblage formed during the circulation of mildly acidic to alkaline waters.

Genesis of the biogenic zone

The minerals found in the red and black rocks, including siderite, calcite, galena, iron monosulphides, and quartz, have not

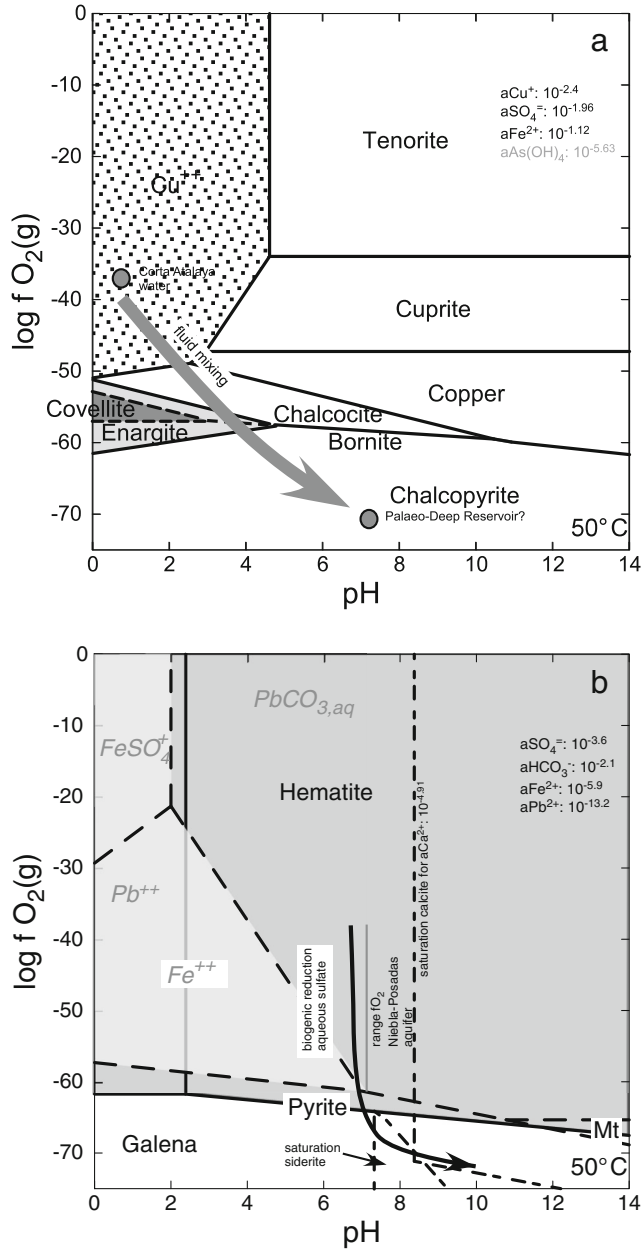

Fig. 12 pH-fO_2 diagrams showing proposed geochemical trends during ore formation at Las Cruces. **a** Advanced cementation zone; covellite stability field is partially replaced by that of enargite, where As is present. Mineralization precipitated by mixing between a fluid, perhaps equivalent to the deep reservoir, and an acidic surficial water, such as that presently filling the Corta Atalaya open pit in Rio Tinto (Sánchez España et al. 2008); **b** Biogenic zone. *Continuous line* limits phases in Pb–S–C–O subsystem and *dashed lines* those of Fe–S–C–O system. Stability constants of enargite are from Spycher and Reed (1989). *mt*, magnetite. Diagrams were calculated assuming activities of solutes in water using an average composition from the deep reservoir and Niebla-Posadas aquifer, at a temperature of 50 °C. Variation of oxygen fugacity of the Niebla-Posadas aquifer is estimated from Eh measured by Scheiber et al. (2015) in the deep zones. These diagrams are only approximate, because the activities of aqueous species change during fluid mixing or fluid-rock reaction, which especially enlarges stability field of siderite in Fig. 14b. Calculated with program GWB of Bethke (2008)

been described in other subaerial gossans. These minerals are unstable under oxidizing subaerial conditions, thus suggesting that the red and black rocks replaced the former gossan when it was buried beneath the Tertiary marl (Fig. 4). The formational conditions of the carbonates are not those expected in gossans, characterized by low fCO_2 and low pH (Taylor and Sylvester 1982). However, secondary galena has been reported in several zones of secondary alteration, especially within the secondary alteration zones of VMS deposits in the Urals (see Belogub et al. 2008).

Replacement of the gossan at Las Cruces implies the following: (1) a redox change involving the reduction of Fe^{3+} to Fe^{2+} associated with the replacement of goethite/hematite by siderite, (2) an increase of fCO_2 that helps to stabilize the carbonates, and (3) an increase of the $aH_2S/aSO_4^{=}$ ratio that produces stable sulphides instead of sulphates and carbonates; the assemblage indicates that the process took place under reduced (anoxic) conditions and a mildly acidic to alkaline pH.

Coupled increases in CO_2 and reduced sulphur in low-temperature aqueous systems are generally related to the simplified reaction under anaerobic conditions that reduces sulphate to sulphide and oxidizes an electron donor. In such systems, different types of low molecular weight organic matter such as methane, hydrocarbons, organic acids, or even $H_{2,g}$ act as electron donors having sulphate as the final electron acceptor and releasing CO_2 and H_2S as byproducts, as follows in the simplified equation:

$$CH_{4,aq} + SO_4^{=} + H^+ <-> HCO_3^- + H_2S_{aq} + H_2O \quad (1)$$

This process also increases the pH (Southam and Saunders 2005) helping to stabilize carbonates. At temperatures below 100–150 °C, the kinetics of abiotic redox reactions, including thermochemical reduction of sulphate, are too sluggish to take place (Ohmoto and Lasaga 1982; Machel 2001). However, consortiums of chemotrophic micro-organisms catalyze these reactions and make them possible at low temperatures (Donald and Southam 1999).

At high pH and low temperature, simplified equations governing the formation of siderite, galena and iron sulphides could be as follows:

$$\text{Goethite} + 2H^+ + CO_3^{=} = \text{Siderite} + 0.25O_2 + 1.5H_2O \quad (2)$$

$$\text{Siderite} + HS^- + Pb^{2+} = \text{Galena} + Fe^{++} + CO_3^{=} + H^+ \quad (3)$$

$$\text{Siderite} + 1.25CH_{4(g)} + 1.33SO_4^{=} = 0.33\text{Greigite} + 2.25CO_3^{=} + 1.83H^+ + 1.58H_2O \quad (4)$$

The main arguments supporting the replacement of a former subaerial gossan by biogenic processes, beneath the sealing cap of marl, include the following: (a) geochemistry of the system, (b) stable isotope geochemistry, and (c) presence of likely bacteriomorphs.

The kinetics of abiotic iron reduction in surficial low-temperature environments are very sluggish, and the reduction of Fe^{3+} to Fe^{2+} is predominantly biotic (Lovley 1997; Neal et al. 2001). Abiogenic reduction of iron has been described only in relationship with photoreduction (Diez Ercilla et al. 2009), and during the oxidation of quinone-rich humic acids and phenoles derived mainly from plant tissues in organic matter-rich settings such as soils (Pracht et al. 2001). Obviously, these mechanisms are not applicable to Las Cruces, where the gossan was replaced some 150 m below the surface. Even in the presence of organic compounds, abiotic iron reduction is significantly less efficient than that produced by prokaryotes (Zehnder and Brock 1980).

The presence of iron monosulphides is indicative of highly reducing conditions and a high Fe^{2+}/S ratio in which the precipitation of pyrite is kinetically inhibited and amorphous or poorly ordered, intermediate compounds of iron sulphide predominate (Kucha and Viaene 1993; Kucha et al. 2005). Elsewhere, these minerals are interpreted as metastable phases that are later replaced by pyrite, pyrrhotite, or marcasite (Hunger and Benning 2007). The presence in the Las Cruces secondary deposit of skeletal, botryoidal, and colloform structures is consistent with rapid precipitation of sulphides in a system that was supersaturated as soon as the reduced sulphur was produced. Despite having been grown in abiotic systems within a laboratory (Furukawa and Barnes 1996), greigite (Fe_3S_4) and smythite ($[Fe,Ni]_{3+x}S_4$) are considered bioproducts in natural systems and their presence is thus indicative of microbial activity (Raiswell and Plant 1980; Kucha et al. 2005; Kucha et al. 2010). The equilibrium between greigite and siderite in this CO_2-rich environment is similar to that described by Furukawa and Barnes (1996), as follows:

$$16\ \text{greigite} + 4\ \text{siderite} + 2H_2 = 4\ \text{smythite} + 4H_2CO_3 \quad (5)$$

which is consistent with the late formation of smythite at Las Cruces. Also, the silver sulphides and gold alloys can be of biogenic origin. Zierenberg and Schiffman (1990) reported the presence of silver sulphides pseudomorphically coating bacteria in mats in present-day submarine-exhalative systems; gold coarsening and precipitation in supergene environments also has been proved to be biologically mediated (Southam et al. 2009; Reith et al. 2010).

The carbon and sulphur isotope composition of the red and black rocks are also consistent with a biogenic derivation of these rocks. Capitán (2006) was the first to find highly depleted $\delta^{13}C$ values in the secondary zone at Las Cruces, but despite interpreting these as linked to biomass concluded that the low values indicated a soil-related origin. Later, Blake (2008) attributed the low $\delta^{13}C$ values to bacteriogenic derivation of the CO_2. The work of Tornos et al. (2014) shows that the $\delta^{13}C$ values of the carbonates reflect the mixing between ^{13}C-enriched carbon ($\delta^{13}C \approx -5‰$), likely inherited from the

dissolved inorganic carbon in the water of the Niebla-Posadas aquifer, and another low-$\delta^{13}C$ carbon reservoir having values lower than −60‰. These late carbon isotope signatures can only be derived by biologically mediated methanotrophy or anaerobic oxidation of methane (AOM) or of low molecular weight organic compounds, precluding the genesis of CO_2 by mechanisms such as biogenic oxidation of $H_{2,g}$, aerobic microbial oxidation of methane, methanogenesis, and abiogenic oxidation (Irwin et al. 1977; Claypool et al. 1985; Spiro et al. 1993; Hornibrook et al. 2000; Polag et al. 2013). The lack of covariation among $\delta^{13}C$ and $\delta^{18}O$ values strongly suggests that the carbon was not transported with H_2O, i.e., it instead was transported as a gas.

The source of the methane or the light organic matter needed for metabolism of the prokaryotes could be the abundant sour gas that is regionally found beneath the marl of the Guadalquivir Basin. The ultimate origin of this gas is unknown, but may derive from the underlying Paleozoic shale of the VS Complex that occurs in the basement of the basin. Thermal maturation of the organic matter-bearing metasediments should release methane that then would ascent along fractures—such as the F1 fault zone—until being accumulated below the sealing marl.

The interpretation of the sulphur isotope data is not straightforward because the measured values are high (galena +11.9 to +25.9‰; iron sulphides +16.3 to +19.5‰; Tornos et al. 2014) and close to the uppermost values of the aqueous sulphate of the Niebla-Posadas aquifer (−13.6 to +21.7‰; Fig. 9 and ESM Table 1). These $\delta^{34}S$ values are uniformly more positive than those of the underlying massive sulphides, indicating that the sulphur present in the biogenic zone is not derived simply by dissolution and later precipitation of the earlier sulphides without isotopic fractionation.

It has been traditionally assumed that biogenic dissimilatory sulphate reduction produces a systematic depletion in $\delta^{34}S$ values of the produced H_2S due to the preferential fractionation of ^{34}S into the remaining sulphate (Ohmoto 1986; Fallick et al. 2001; Bawden et al. 2003). However, this result is not always correct because biogenically mediated sulphate reduction is not always associated with a large $\Delta^{34}S_{SO4\text{-}H2S}$. Possible reasons include the following: (a) the nature of the extremophilic microorganisms. Experiments have shown that not all sulphate-reducing prokaryotes significantly fractionate sulphur isotopes, a process that depends greatly on their specific physiology (Detmers et al. 2001; Kleikemper et al. 2004); (b) the type and amount of nutrients as well as the formation of intermediate compounds, or the final released products, also exert a strong influence on $\Delta^{34}S_{sulphate\text{-}sulphide}$ values (Rudnicki et al. 2000; Detmers et al. 2001; Habicht and Canfield 2001; Hoek et al. 2004; Brunner and Bernasconi 2005). In general, systems having excess electron donors (e.g., H_2, CH_4, or organic matter>>$SO_4^{=}$) tend to produce reduced sulphur with low $\Delta^{34}S_{sulphate\text{-}sulphide}$ values that can be as low as −1.5‰ (Paytan 2000); (c) the rate of sulphate reduction in which the degree of fractionation is inversely proportional to the rate; and (d) the open or closed nature of the system for sulphate or sulphide. The compilation of (Ohmoto 1986; see also Goldhaber and Kaplan 1974) shows that in systems closed to sulphate, Rayleigh fractionation controls the isotope composition of the resulting reduced sulphur; hence, the precipitated sulphides can have $\delta^{34}S$ values similar to those of the original aqueous sulphate (Goldhaber and Kaplan 1980; Strauss and Schieber 1990; Rudnicki et al. 2000; Southam and Saunders 2005; Johnson et al. 2009). Thus, we disagree with the widely used statement that high $\delta^{34}S_{sulphide}$ values rule out sulphate reduction as being related to the metabolism of sulphate-reducing prokaryotes. It is more scientifically correct to say that large $\delta^{34}S$ depletions suggest biogenic reduction of sulphate but the opposite is not necessarily true. Therefore, the lack of significant observed $\Delta^{34}S_{sulphate\text{-}sulphide}$ fractionations in no way indicates the absence of biogenic sulphate reduction. Simply stated, BSR cannot be traced isotopically because the $\delta^{34}S$ values may mask those of magmatic or TSR derivation.

In the case of the biogenic zone, the sulphur isotopes and mineralogy suggest that the limiting factor for biogenic activity was not the deficiency of electron donors but rather the availability of enough sulphate. We hypothesize that the aqueous sulphate supplied by the aquifer was quickly reduced in a system having excess methane or hydrocarbons, and closed to H_2S due to the significant availability of metals that promoted rapid precipitation of the sulphides (Tornos et al. 2014). However, the fact that $\delta^{34}S_{sulphide}$ values of the biogenic zone only match the highest $\delta^{34}S_{SO4}$ values of the aquifer can only be explained by the isotopically heaviest end-member having dominated the system during secondary mineralization.

One of the most striking features of the Las Cruces deposit is the presence of lenses of up to 2–3 m thick of nearly monomineralic galena in the footwall of the black rock. These lenses are probably recrystallized microbial colonies in where galena saturated due to the local increase of the aH_2S related to the metabolism of sulphate-reducing microbes. In order to constrain the formation of this galena, we present geochemical diagrams that track the evolution of fluids and minerals in the deposit. Figure 13 is a simplified plot of the solubility of Pb and precious metals where the gossan interacts with the water of the Niebla-Posadas aquifer, in a progressively reducing system and a pH buffered by the fluid. Under oxidizing conditions, the first batches of water are able to dissolve significant amounts of lead, mostly transported as $PbCO_{3(aq)}$, but lead mobility decreases greatly under more reducing conditions; these calculations are consistent with the low lead contents in the Niebla-Posadas aquifer (Table 2). This evolution probably explains why lead is concentrated predominantly in the base of the biogenic zone—it dissolved in the more oxidized parts and precipitated in the

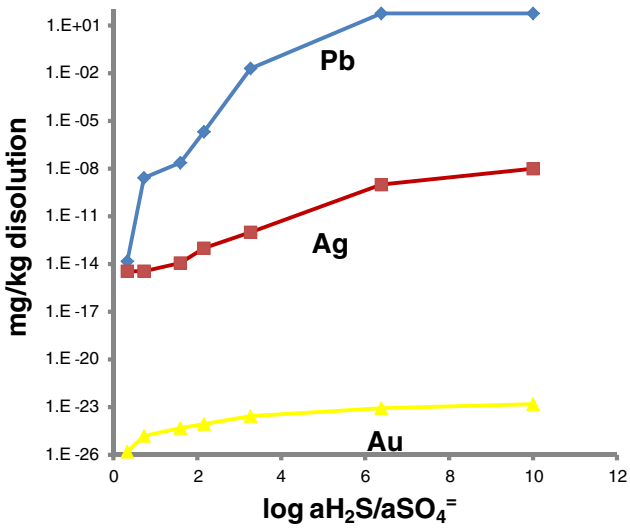

Fig. 13 Relationship between the solubility of the metals enriched in the biogenic zone and the redox state (as $aH_2S/aSO_4^=$) of the system

euxinic ones, in equilibrium with the iron monosulphides in the bottom of the system; also explained is why secondary galena can be found within fractures in the massive sulphides and overlying marl. However, these results additionally show that the solubilities of both gold and silver are very low, below 10^{-8} μg/g. Thus, these metals should behave basically as inert components unless other non-considered aqueous complexes are involved. Figure 12b shows the proposed evolution in fO_2-pH space during the reaction of the Niebla-Posadas aquifer water with the early gossan, synchronous with the biogenic reduction of aqueous sulphate. The predicted trend matches the observed mineralogy, including the formation of iron sulphides (assumed to be thermodynamically equivalent to metastable iron sulphides) and galena, accompanied by the early precipitation of siderite followed by calcite.

Thus, the geology and geochemistry of the red and black rocks likely track the existence of a giant, deep, subsurface bioreactor where the metabolism of extremophilic prokaryotes has modified the mineralogy of million tons of ore (Tornos et al. 2014). Here, coupled iron reduction-sulphate reduction-X_{CO2} increase were kinetically favored by the metabolism of competing communities of chemolithotrophic prokaryotes, their activity being limited by the presence of water, suitable temperature, and availability of nutrients (Southam and Saunders 2005). It is likely that this process was complex and involved alternating events of major biogenic growth and partial oxidation that may have corresponded to seasonal or hydrologic variations, which would explain the observed isotopic changes (Fortin and Beveridge 1997). The presence of late goethite replacing the siderite is probably related to fluctuations in the composition of the water within the aquifer. These prokaryotes catalyze reaction rates and can form unstable or metastable assemblages that are otherwise not stable under supergene conditions (Shock 2009). The formation of the biogenic zone is controlled by the existence of a large aquifer crosscutting a highly porous gossan below the sealing marl, and adjacent to pathways for ascending methane. If the model of Scheiber et al. (2015) is correct in proposing that the Niebla-Posadas aquifer hosts regional biogenic sulphate reduction, the inferred bioreactor must have been significantly larger than the Las Cruces orebody. However, the presence of fossils of bacteria replaced by galena at Las Cruces (Tornos et al. 2014) indicates that at least some saturation in reduced sulphur was attained in situ.

Yesares et al. (2014) suggested that the red and black rocks formed by reaction of downward-percolating fluids with the gossan but without mention of possible biological involvement. However, the later work of Yesares et al. (2015) states that other factors such as biological activity must be considered in order to explain the mineralogical and isotopic data for Las Cruces, but criticizes the bio-reactor model. In their model, the source of sulphate, CO_2, and methane needed for the formation of the gossan and the epithermal veins is not the Niebla-Posadas aquifer or gasses ascending along faults, but rather downward-percolating waters that descended through more than 150 m of Tertiary marl. This interpretation is at odds with the isotope data, however, which show the O–H–C–Sr signatures of the biogenic zone, the epithermal veins, and the groundwater are significantly different from those of the Tertiary marl (Figs. 7, 8, and 9), thus indicating that the ore-forming fluids, and hence those of the Niebla-Posadas aquifer, have not equilibrated with the Tertiary sediments. Also, we consider it unlikely that fluids could gravitationally percolate through this essentially impermeable sequence that independently has been shown to be a low-transmissivity sealing cap for the confined Niebla-Posadas aquifer (Scheiber et al. 2015). Furthermore, the solubility of methane in water at the expected low temperatures (<50 °C) and quasi-hydrostatic fluid pressures in this environment is very low (ca. 0.015–0.02 g/kg H_2O). Also, transport in a gas is inconsistent with the geological evidence that a low-density phase such as methane gas would percolate downwards through a relatively high-density sedimentary sequence. Thus, an abiotic origin is at odds with available geological and geochemical data, as well as with the presence of microfossils of prokaryotes within the black rock (Tornos et al. 2014). Also, Yesares et al. (2015) proposed a similar descending model for the lead enrichment in the Las Cruces deposit but in their model the trap is attributed to a layer of black shale located between the gossan and the cementation zone. As discussed above, we have not found any evidence of such a shale and therefore we interpret all of the black rock to be a product of the metasomatic replacement of the gossan.

The source of heat

There is no record in the Las Cruces area of young igneous rocks that could be coeval with the secondary mineralization or evidence of post-Variscan magmatism in the Guadalquivir

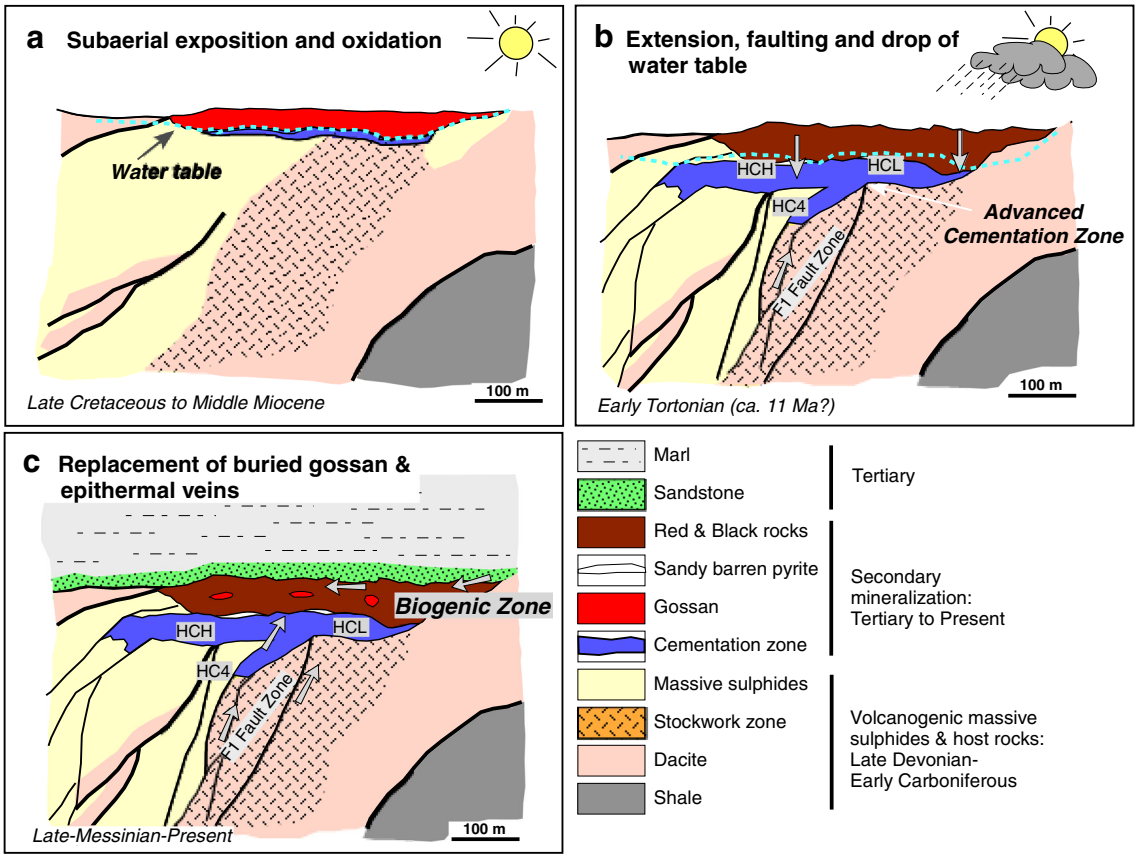

Fig. 14 Simplified genetic model of the Alpine evolution of the Las Cruces deposit showing the direct relationship of the high-grade ore and the Biogenic Zone with the Alpine extension and maturation beneath a sealing cap

Basin. However, and as noted above, waters currently upwelling into the Las Cruces open pit have anomalously high temperatures of 18 to 43 °C (Table 2). Both the advanced cementation zone and the epithermal veins show widespread evidence of having been formed, at least episodically, at temperatures between 100 and 150 °C. These temperatures are clearly high for a typical supergene environment. For comparison, fluid inclusion studies in some gossans have yielded temperatures up to 85 °C (Foley and Flohr 1998), which probably reflect the exothermic oxidation of pyrite under low fluid/rock ratios in the unsaturated (vadose) zone (Sracek et al. 2006). Similarly, Melchiorre et al (1999) also noted that the groundwater temperatures recorded by carbonate mineral thermometers during secondary enrichment in massive sulphide districts are up to 20 °C greater than for disseminated deposits. However, the lack of oxidized pyrite beneath the Las Cruces secondary deposit excludes such an alternative. Knight (2000) previously noted the presence of an abnormal high heat flow at Las Cruces, proposing that during burial there was an increase in the geothermal gradient and consequently a marked change in the sulphide mineral assemblage, including the late replacement of digenite by bornite and chalcopyrite.

Our interpretation is that the high heat flow was related to basin extension and crustal thinning that has taken place in the study area since Miocene times—sometimes leading to widespread mafic magmatism as can be seen in the western Mediterranean region from 6.3 to 0.65 Ma (e.g., Duggen et al. 2005; Lustrino and Wilson 2007). Currently active in the Guadalquivir Basin are several low-enthalpy geothermal fields that have sub-economic potential; the upper aquifer is between 1000 and 2000 m deep, with heat fluxes above 90 mW/m² and present-day temperatures near 100 °C (Albert 1979; Fernández et al. 1998). It is likely that during maximum basin extension in the Messinian, thermal gradients were higher than today and episodic bursts of groundwater had sufficiently high enthalpy to boil near the surface. This heated groundwater, which we propose flowed along structures such as the F1 fault, was responsible for forming the advanced cementation zone and the epithermal veins. However, the elevated temperatures that existed during the Messinian have probably declined through time and now are much lower.

Conclusions: an integrated geological model

The high copper grades and unusual mineralogy of the secondary Las Cruces deposit are here interpreted as being genetically related to post-Miocene processes. These processes

involve evolution of the mineralization by accelerated growth of the secondary zone due to extensional tectonics and later burial, which together formed two types of ore assemblages that are uncommon in secondary ore deposits elsewhere (Fig. 14). The primary VMS deposit and an early capping supergene (cementation/gossan) alteration zone were affected by a younger polyphase (sub)surficial alteration that produced a complex, high-grade advanced cementation zone characterized by pervasive replacements and large veins of massive chalcocite with coeval acid alteration zones. This advanced cementation zone formed during the accelerated evolution and collapse of the subaerial supergene profile, related to extensional faulting linked to basin configuration and a concomitant lowering of the water table. The advanced cementation zone shows evidence of abnormally high temperatures that are here attributed to regional high heat flow; this zone formed due to the mixing of descending, acidic, Cu-bearing oxidized groundwater with upwelling, relatively hot (>100 °C), alkaline water along extensional faults. The development of this large and high-grade cementation zone was likely accompanied by formation of a major gossan that was eroded before being covering by sediments related to the Messinian transgression (ca. 7.2 Ma), a process that interrupted the weathering and oxidation of the deposit. Three Ar-Ar ages of the altered volcanic rocks suggest that the supergene alteration could occur episodically at ≈85.6 Ma (Late Cretaceous), ≈63.5 Ma (Early Paleocene), and 45.5 ± 2.4 Ma (Early Eocene), but that the advanced cementation zone formed much later over a short time span of less than 0.7 m.y. in the early Tortonian (11.2 ± 0.2 to 10.8 ± 0.1 Ma).

After burial, the deposit continued its geochemical evolution. This evolution was controlled by the dramatic change in composition of the water existing in the top of the basement, which changed from acidic groundwater to a SO_4-bearing but more alkaline and CO_2-rich groundwater—likely similar to that flowing through the present-day Niebla-Posadas aquifer. Fluid mixing with hot, deep, alkaline, Na-rich water and intermittent boiling produced epithermal-type quartz-calcite-barite veins and breccias accompanied by remobilization of Cu-Fe-(As) sulphides. In the upper part of this system, there was widespread precipitation of silica and the formation of a silica-rich zone.

The post-burial conditions lead to the formation of a giant bioreactor. Remnants of the buried gossan, located along the basement-cover contact, trapped sour gas that likely upwelled along extensional faults and were saturated by groundwater of the Niebla-Posadas aquifer in a confined environment isolated from the atmosphere. These conditions favored the development of a flourishing, large, extremophilic microbial ecosystem that was responsible for widespread CO_2 generation and sulphate reduction, and for gradual replacement of the gossan by an unusual mineral assemblage dominated by carbonates, galena, and iron monosulphides under gradually more reducing conditions (biogenic zone). The evolution of the system was probably marked by a balance in the flux between deep water and that from the Niebla-Posadas aquifer, the oxic/anoxic interface, and elevated heat flow, which in concert were likely controlled by tectonic activity, far-field mafic magmatism, and perhaps the cycles of wet and dry seasons.

Acknowledgments This study was funded by the Spanish project SEIDI CGL 2011-23207 to FT and FV, the grant IT762-13 (GIC12/104) of the Basque Government to FV and, in its initial stages, by ProMine EU project FP7-NMP-2008-LARGE-2 228559. We would like to thank Cobre Las Cruces SA (First Quantum Minerals) for granting access to the open pit mine and allowing sampling of drill cores and waters. Special thanks are given to Ivan Carrasco, Juan Carlos Baquero, Antonio Francos, José Gómez, and Gobain Obejero for continuous support and sharing knowledge of the mine. We also acknowledge Carmen Conde, Cesar Menor, and Juan Carlos Videira for fruitful discussions and advice on the geology and mineralogy of the deposit. We additionally thank Carlos Ayora (CSIC), Baruch Spiro (Natural History Museum, London), and Ricardo Amils, Monika Oggerin, Nuria Rodriguez, and Enoma Omoregie (all Centro de Astrobiología, CSIC-INTA) for comments and suggestions on geomicrobiology, Clemente Recio (Universidad de Granada) for help in the stable isotope data, and Terry Spell for suggestions on interpretation of the Ar-Ar ages. We are also indebted to the technicians from the laboratories (including Sgiker of the University of the Basque Country) for their help with the analyses presented in this research. Finally, we thank Erik Melchiorre, Albert Gilg, and Bernd Lehmann for the thoughtful review and editing of the manuscript.

References

Ague JJ, Brimhall GH (1989) Geochemical modeling of steady state fluid flow and chemical reaction during supergene enrichment of porphyry copper deposits. Econ Geol 84:506–528

Al-Aasm IS, Taylor BE, South B (1990) Stable isotope analysis of multiple carbonate samples using selective acid extraction. Chem Geol 90:119–125

Albert JF (1979) El mapa español de flujos caloríficos. Intento de correlación entre anomalías geotérmicas y estructura cortical. Bol Geol Min 90:36–48

Almodovar GR, Castro JA, Sobol F, Toscano M (1997) Geology of the Rio Tinto ore deposits Geology and VMS deposits of the Iberian Pyrite Belt. SEG Fieldbook Series 27: pp 165-172

Almodovar GR, Saez R, Pons JM, Maestre A, Toscano M, Pascual E (1998) Geology and genesis of the Aznalcollar massive sulphide deposits, Iberian Pyrite Belt, Spain. Mineral Deposita 33:111–136

Alpers CH, Brimhall GE (1989) Paleohydrologic evolution and geochemical dynamics of cumulative supergene metal enrichment at La Escondida, Atacama Desert, Northern Chile. Econ Geol 84:229–255

Alvaro A (2010) Mineralogía y geoquímica de sulfatos secundarios en ambientes de drenaje ácido de mina. Área minera del yacimiento de San Miguel (Faja Pirítica Ibérica). PhD Thesis, Universidad Pais Vasco, pp 273

Anderson JA (1982) Characteristics of leached capping and techniques of appraisal. In: Advances in the geology of porphyry copper deposits; southwestern North America. University Arizona Press, Tucson, pp 275–295

Arribas A (1995) Characteristics of high-sulfidation epithermal deposits and their relation to magmatic fluid. Min Assoc Can Short Course 23:419–454

Barrie CT, Amelin Y, Pascual E (2002) U-Pb geochronology of VMS mineralization in the Iberian Pyrite Belt. Mineral Deposita 37:684–703

Barriga FJAS (1990) Metallogenesis in the Iberian Pyrite Belt. In: Dallmeyer RD, Martinez Garcia E (eds) Pre-Mesozoic geology of Iberia. Springer Verlag, Heidelberg, pp 369–379

Barton PB, Skinner BJ (1979) Sulfide mineral stabilities. In: Barnes HL (ed) Geochemistry of hydrothermal ore deposits, 2nd edn. Wiley, New York, pp 278–240

Baumgartner R, Fontboté L, Vennemann T (2008) Mineral zoning and geochemistry of epithermal polymetallic Zn-Pb-Ag-Cu-Bi mineralization at Cerro de Pasco, Peru. Econ Geol 103:493–537

Bawden TM, Einaudi MT, Bostick BC, Meibom A, Wooden J, Norby JW, Orobona MJT, Chamberlain CP (2003) Extreme S-34 depletions in ZnS at the Mike gold deposit, Carlin Trend, Nevada: evidence for bacteriogenic supergene sphalerite. Geology 31:913–916

Belogub EV, Novoselov CA, Spiro B, Yakovleva BA (2003) Mineralogical and S isotopic features of the supergene profile of the Zapadno-Ozernoe massive sulphide and Au-bearing gossan deposit, South Urals. Mineral Mag 67:339–354

Belogub EV, Novoselov KA, Yakovleva VA, Spiro B (2008) Supergene sulphides and related minerals in the supergene profiles of VHMS deposits from the South Urals. Ore Geol Rev 33:239–254

Bendezú R, Fontboté L (2009) Cordilleran epithermal Cu-Zn-Pb-(Au-Ag) mineralization in the Colquijirca District, Central Peru: deposit-scale mineralogical patterns. Econ Geol 104:905–944

Bethke CM (2008) Geochemical and biogeochemical modeling. Cambridge University Press, 543 p

Blake C (2008) The mineralogical characterisation and interpretation of a precious metal-bearing fossil gossan, Las Cruces, Spain. Ph D Thesis, Cardiff University, pp 207

Boyle DR (2003) Preglacial weathering of massive sulfide deposits in the Bathurst Mining Camp: economic geology, geochemistry, and exploration applications In: Goodfellow WD, McCutcheon SR, Peter JM (eds) Massive sulphide deposits of the Bathurst Mining Camp, New Brunswick, and Northern Maine. Soc Explor Geophys, Geophys Monogr 11: 689–721

Braxton DP, Cooke DR, Ignacio AM, Rye RO, Waters PJ (2009) Ultra-deep oxidation and exotic copper formation at the Late Pliocene Boyongan and Bayugo porphyry copper-gold deposits, Surigao, Philippines: geology, mineralogy, paleoaltimetry, and their Implications for geologic, physiographic, and tectonic controls. Econ Geol 104:333–349

Brimhall GH, Alpers CN, Cunningham AR (1985) Analysis of supergene ore forming processes and groudwater solute transport using mass balance principles. Econ Geol 80:1227–1256

Brunner B, Bernasconi SM (2005) A revised isotope fractionation model for dissimilatory sulfate reduction in sulfate reducing bacteria. Geochim Cosmochim Acta 69:4759–4771

Capitán MA (2006) Mineralogía y geoquímica de la alteración superficial de depósitos de sulfuros masivos en la Faja Pirítica Ibérica. PhD Thesis, Universidad de Huelva, 360 p.

Capitán MA, Nieto JM, Saez R, Almodovar GR (2004) Mineralogía del gossan del yacimiento de Las Cruces (Sevilla). Macla 2:21–22

Carothers WW, Adami LH, Rosenbauer RJ (1988) Experimental oxygen isotope fractionation between siderite-water and phosphoric acid liberated CO_2-siderite. Geochim Cosmochim Acta 52:2445–2450

Carvalho D, Barriga FJAS, Munha J (1999) Bimodal siliciclastic systems—the case of the Iberian Pyrite Belt. Rev Econ Geol 8:375–408

Chipera SJ, Apps JA (2001) Geochemical stability of natural zeolites. Rev Mineral Geochem 45:117–161

Civis J, Sierro FJ, González-Delgado JA, Flores JA, Andrés I, Porta J, Valle MF (1987) El Neógeno marino de la provincia de Huelva, antecedentes y definición de las unidades litoestratigráficas. In: Paleontología del Neógeno de Huelva (W del Guadalquivir). Ediciones Universidad de Salamanca. pp 9–27

Claypool GE, Holser WT, Kaplan IR, Sakai H, Zak I (1980) The age curves of sulfur and oxygen isotopes in marine sulfate and their mutual interpretation. Chem Geol 28:199–260

Claypool GE, Threlkeld C, Mankiewicz P, Arthur M, Anderson TF (1985) Isotopic composition of interstitial fluids and origin of methane in slope sediment of the Middle America trench, Deep-Sea Drilling Project Leg-84. Initial Rep Deep Sea Drill Proj 84:683–691

Conde C, Tornos F, Fernandez J, Doyle M (2003) Encuadre estratigráfico de los sulfuros masivos de la parte Suroriental de la Faja Piritica: Aznalcollar-Los Frailes y Las Cruces. Bol Sociedad Española Mineralogía 26-A:161–162

Conde C, Tornos F, Doyle M et al (2007) Geology and lithogeochemistry of the unique Las Cruces VMS deposit, Iberian Pyrite Belt. In: Andrew CJ (ed) Digging deeper. Proceedings of the 9th Biennial SGA Meeting IAEG, Dublin, pp 1101–1104

Deer WA, Howie RA, Zussman J (1966) Rock forming minerals. Longman Press, London

Detmers J, Brüchert V, Habicht KS, Kuever J (2001) Diversity of sulfur isotope fractionations by sulfate-reducing prokaryotes. Appl Environ Microbiol 67:888–894

Diez Ercilla M, López Pamo E, Sánchez España J (2009) Photoreduction of Fe(III) in the acidic mine pit lake of San Telmo (Iberian Pyrite Belt): field and experimental work. Aquat Geochem 15:391–419

Donald R, Southam G (1999) Low temperature anaerobic bacterial diagenesis of ferrous monosulfide to pyrite. Geochim Cosmochim Acta 63:2019–2023

Doyle M (1996) Las Cruces copper proyect, Pyrite Belt, Spain. Bol Geol Min 107:681–683

Doyle M, Morrissey C, Sharp G (2003) The Las Cruces Orebody, Seville province, Andalucía, Spain. In: Kelly CG, Andrew CJ, Ashton JH, Boland MB, Earls G, Fusciardi L, Stanley G (eds) The geology and genesis of Europe's major base metal deposits. Irish Association for Economic Geology, Dublin, pp 381–390

Duggen S, Hoernle K, van den Bogaard P, Garbe-Schönberg D (2005) Post-collisional transition from subduction-to intraplate-type magmatism in the westernmost Mediterranean: evidence for continental-edge delamination of subcontinental lithosphere. J Petrol 46:1155–1201

Emmons WH (1918) The principles of economic geology. McGraw-Hill Book Company

Epstein S, Mayeda TK (1953) Variation of the $^{18}O/^{16}O$ ratio in natural waters. Geochim Cosmochim Acta 4:213–224

Fallick AE, Ashton JH, Boyce AJ, Ellam RM, Russell MJ (2001) Bacteria were responsible for the magnitude of the world class hydrothermal base metal sulfide orebody at Navan, Ireland. Econ Geol 96:885–890

Fernández M, Berástegui X, Puig C, García-Castellanos D, Jurado MJ, Torné M, Banks C (1998) Geophysical and geological constraints on the evolution of the Guadalquivir foreland basin, Spain. Geol Soc Lond Spec Publ 134:29–48

Foley NK, Flohr MJK (1998) Ancient gossan formation at the Bald Mountain VMS deposit, Maine: a natural analogue of the modern oxidation of tailing piles? GSA Meeting. Abstr with programs 29: A166

Fortin D, Beveridge T (1997) Microbial sulfate reduction within sulfidic mine tailings: formation of diagenetic Fe sulfides. Geomicrobiol J 14:1–21

Friedman I, O'Neil JR (1977) Data of Geochemistry. Compilation of stable isotope fractionation factors of geochemical interest USGS Professional Paper 440-KK, 12 pp

Furukawa Y, Barnes HL (1996) Reactions forming smythite, Fe_9S_{11}. Geochim Cosmochim Acta 60:3581–3591

Galán E, González L, Mayoral E, Muñiz F (1995) Contribution of clay mineralogy to the paleoenvironmental interpretation of upper miocene detrital sediments. Southwestern of the Iberian Peninsula In: Elsen P, Grobet M, Keung H, Leeman R, Schoonheydt R, Toufar H (eds) Euroclay'95. Leuveil, pp 311–312

Galindo C, Pankhurst RJ, Casquet C, Coniglio J, Baldo E, Rapela CW, Saavedra J (1997) Age, Sr- and Nd-isotope systematics and origin of two fluorite lodes, Sierras Pampeanas, Argentina. Int Geol Rev 39: 948–954

Gaspar OC (2002) Mineralogy and sulfide mineral chemistry of the Neves Corvo ores, Portugal: insight into their genesis. Can Min 40:611–636

Goldhaber MB, Kaplan IR (1974) The sulfur cycle. In: Goldberg ED (ed) The sea. Wiley, New York, pp 569–655

Goldhaber MB, Kaplan IR (1980) Mechanisms of sulfur incorporation and isotope fractionation during early diagenesis in sediments of the Gulf of California. Mar Chem 9:95–143

Gonzalez F, Moreno C, Saez R, Clayton J (2002) Ore genesis age of the Tharsis Mining District (Iberian Pyrite Belt): a palynological approach. J Geol Soc Lond 159:229–232

Grenne T, Slack JF (2003) Bedded jaspers of the Ordovician Løkken ophiolite, Norway: seafloor deposition and diagenetic maturation of hydrothermal plume-derived silica-iron gels. Mineral Deposita 38:625–639

Habicht KS, Canfield DE (2001) Isotope fractionation by sulfate-reducing natural populations and the isotopic composition of sulfide in marine sediments. Geology 29:555–558

Hedenquist JW, Simmons SF, Giggenbach WF, Eldridge CW (1993) White Island, New Zealand, volcanic-hydrothermal system represents the geochemical environment of high sulfidation Cu and Au ore deposition. Geology 21:731–734

Henley RW, Truesdell AH, Barton PB, Whitney JA (1984) Fluid-mineral equilibria in hydrothermal systems. Rev Econ Geol 2; 267 p

Heyl AV (1964) Enargite in zinc-lead deposits of Upper Mississippi Valley district. Am Mineral 49:1458

Hoek J, Reysenbach A, Habicht K, Canfield DE (2004) The effect of temperature and hydrogen limited growth on the fractionation of sulfur isotopes by *Thermodesulfatator indicus*, a deep-sea hydrothermal vent sulfate-reducing bacterium. Trans AGU 85:B21A–0857

Hornibrook ER, Longstaffe FJ, Fyfe WS (2000) Evolution of stable carbon isotope compositions for methane and carbon dioxide in freshwater wetlands and other anaerobic environments. Geochim Cosmochim Acta 64:1013–1027

Hunger S, Benning LG (2007) Greigite: a true intermediate on the polysulfide pathway to pyrite. Geochem Trans 8:1

IAEA (2015) WISER: Water Isotope System for Data Analysis, Visualization and Electronic Retrieval. http://www.naweb.iaea.org/napc/ih/IHS_resources_isohis.html. Accessed Feb 2015

IGME (1983) Hidrogeología del Parque Nacional de Doñana y su entorno. Instituto Geológico y Minero de España, Madrid, **120 p**

IGME (2010) Mapa Geológico de España E: 1/200000 Sevilla-Puebla de Guzman (75-74)

Irwin H, Curtis C, Coleman M (1977) Isotopic evidence for source of diagenetic carbonates formed during burial of organic-rich sediments. Nature 269:209–213

Johnson CA, Emsbo P, Poole FG, Rye RO (2009) Sulfur- and oxygen-isotopes in sediment-hosted stratiform barite deposits. Geochim Cosmochim Acta 73:133–147

Kleikemper MH, Schroth SM, Bernasconi B, Brunner R, Zeyer J (2004) Sulfur isotope fractionation during growth of sulfate reducing bacteria on various carbon sources. Geochim Cosmochim Acta 23: 4891–4904

Knight FC (2000) The mineralogy, geochemistry and genesis of the secondary sulphide mineralisation of the Las Cruces, Spain. PhD Thesis, University of Cardiff, pp 434

Knight FC, Rickard D, Boyce AJ (1999) Multigenic origin for secondary enrichment in Las Cruces VMS deposit, Iberian Pyrite Belt In: Stanley et al. (eds) Mineral deposits: Processes to Processing. Balkema, pp 543-546

Kojima S, Trista-Aguilera D, Hayashi K (2009) Genetic aspects of the manto-type copper deposits based on geochemical studies of North Chilean deposits. Resour Geol 59:87–98

Kosakevitch A, Palomero F, Leca X, Leistel J, Lenotre N, Sobol F (1993) Climatic and geomorphological controls on the gold concentrations of the Rio-Tinto gossans (Huelva province, Spain). CR Academie Sciences Serie II 316:85-90

Kucha H, Viaene W (1993) Compounds with mixed and intermediate sulfur valences as precursors of banded sulfides in carbonate-hosted Zn-Pb deposits in Belgium and Poland. Mineral Deposita 28:13–21

Kucha H, Schroll E, Stumpfl EF (2005) Fossil sulphate-reducing bacteria in the Bleiberg lead-zinc deposit, Austria. Mineral Deposita 40:123–126

Kucha H, Schroll E, Raith JG, Halas S (2010) Microbial Sphalerite formation in carbonate-hosted Zn-Pb ores, Bleiberg, Austria: micro- to nanotextural and sulfur isotope evidence. Econ Geol 105:1005–1023

Large RR (1992) Australian volcanic-hosted massive sulfide deposits: features, styles and genetic models. Econ Geol 87:471–510

Leach DL, Viets JB, Foley-Ayuso N, Klein DP (1995) Mississippi Valley-type Pb-Zn deposits. Preliminary compilation of descriptive geoenvironmental mineral deposit models US Geological Survey Open-File Report 95-831: 234–243

Leistel JM, Marcoux E, Thieblemont D, Quesada C, Sanchez A, Almodovar GR, Pascual E, Saez R (1998) The volcanic-hosted massive sulphide deposits of the Iberian Pyrite Belt. Review and preface to the special issue. Mineral Deposita 33:2–30

Leverett P, McKinnon AR, Williams PA (2005) Supergene geochemistry of the Endeavor ore body, Cobar, NSW, and relationships to other deposits in the Cobar Basin. Proceedings Regolith 2005, p. 191–194

Lovley DR (1997) Microbial Fe(III) reduction in subsurface environments. FEMS Microbiol Rev 20:305–313

Lustrino M, Wilson M (2007) The circum-Mediterranean anorogenic Cenozoic igneous province. Earth Sci Rev 81:1–65

Machel HG (2001) Bacterial and thermochemical sulfate reduction in diagenetic settings—old and new insights. Sediment Geol 140: 143–175

Manzano M, Soler A, Carrera J, Custodio E (2004) Estudio Isotópico del Origen del Sulfato del Agua Subterránea en la Zona Afectada por el Vertido Minero de Aznalcóllar (SO España). Seminarios Sociedad Española de Mineralogía 1:71–88

May ER (1977) Flambeau: a Precambrian supergene enriched massive sulfide deposit. University of Wisconsin, Geological and Natural History Survey 24 p

McCrea JM (1959) On the isotopic chemistry of carbonates and the paleotemperature scale. J Phys Chem 18:849–857

Melcher F, Oberthur T, Rammlmair D (2006) Geochemical and mineralogical distribution of germanium in the Khusib Springs Cu-Zn-Pb-Ag sulfide deposit, Otavi Mountain Land, Namibia. Ore Geol Rev 28:32–56

Melchiorre EB, Enders MS (2003) Stable isotope geochemistry of copper carbonates at the Northwest Extension Deposit, Morenci district, Arizona: implications for conditions of supergene oxidation and related mineralization. Econ Geol 98:607–621

Melchiorre EB, Williams PA (2001) Stable isotope characterization of the thermal profile and subsurface biological activity during oxidation of the Great Australia deposit, Cloncurry, Queensland, Australia. Econ Geol 96:1685–1693

Melchiorre EB, Criss RE, Rose TP (1999) Oxygen and carbon isotope study of natural and synthetic malachite. Econ Geol 94:245–259

Melendez-Hevia E, Alvarez del Buergo E (1996) Oil and gas resources of the Tertiary basins of Spain In: Friend PF, Dabrio CJ (eds) Tertiary Basins of Spain: The Stratigraphic Record of Crustal Kinematics. Cambridge University Press, pp 20-23

Menor C, Tornos F, Fernandez Remolar D, Amils R (2010) Association between catastrophic paleovegetation changes at the Devonian-Carboniferous boundary and the formation of giant massive sulfide deposits. Earth Planet Sci Lett 299:398–408

Miguelez NG, Tornos F, Velasco F, Videira JC (2011) The unusual supergene Las Cruces copper ore deposit. In: Barra F, Reich M, Campos E, Tornos F (eds) SGA Biennial Meeting Proceedings: Let's talk Ore Deposits. Antofagasta, pp 832–834

Miguélez NG, Mathur R, Tornos F, Velasco F, Cooper S (2012a) A copper isotope study in the rich Las Cruces ore deposit to trace a new mineralization style in the Iberian Pyrite Belt. Min Mag 75:1467

Miguélez NG, Mathur R, Tornos F, Velasco F, Cooper S (2012b) A copper isotope study of the Las Cruces ore deposit and its comparison with Rio Tinto and Tharsis mineralizations of the Iberian PyriteBelt (SW Spain). Abstracts SEG Conference, Lima

Moreno C (1993) Postvolcanic paleozoic of the Iberian Pyrite Belt: an example of basin morphologic control on sediment distribution in a turbidite basin. J Sediment Petrol 63:1118–1128

Moreno C, Sierra S, Saez R (1996) Evidence for catastrophism at the Famennian-Dinantian boundary in the Iberian Pyrite Belt. In: Strogen P, Somervilee ID, Jones GL (eds) Recent advances in Lower Carboniferous Geology. Geol Soc London, pp 153–162

Moreno C, Capitan MA, Doyle M, Nieto JM, Ruiz F, Saez R (2003) Edad mínima del gossan de Las Cruces: implicaciones sobre la edad del inicio de los ecosistemas extremos en la Faja Pirítica Ibérica. Geogaceta 33:67–70

Morris RC, Fletcher AB (1987) Increased solubility of quartz following ferrous-ferric iron reactions. Nature 330:558–561

Neal AL, Techkarnjanaruk S, Dohnalkova A, McCready D, Peyton BM, Geesey GG (2001) Iron sulfides and sulfur species produced at hematite surfaces in the presence of sulfate-reducing bacteria. Geochim Cosmochim Acta 65:223–235

Ohmoto H (1986) Stable isotope geochemistry of ore deposits stable isotopes in high temperature geological processes. Rev Mineral 16:491–555

Ohmoto H, Lasaga A (1982) Kinetics of reactions between aqueous sulfates and sulfides in hydrothermal systems. Geochim Cosmochim Acta 46:1727–1745

Oliveira JT (1990) South Portuguese zone: introduction. Stratigraphy and synsedimentary tectonism. In: Dallmeyer RD, Martinez García E (eds) Premesozoic geology of Iberia. Springer Verlag, Heidelberg, pp 333–347

Oliveira V, Matos J, Bengala M, Silva N, Suosa P, Torres L (1998) Geology and geophysics as successful tools in the discovery of the Lagoa Salgada orebody (Sado Tertiary Basin-Iberian Pyrite Belt), Grandola, Portugal. Mineral Deposita 33:170–187

Oliveira DPS, Matos JX, Rosa CJP, Rosa DRN, Figueiredo MO, Silva TP, Guimaraes F, Carvalho JRS, Pinto AMM, Relvas JRMS, Reiser FKM (2011) The Lagoa Salgada Orebody, Iberian Pyrite Belt, Portugal. Econ Geol 106:1111–1128

Onezime J, Charvet J, Faure M, Chauvet A, Panis D (2002) Structural evolution of the southernmost segment of the West European Variscides: the South Portuguese Zone (SW Iberia). J Struct Geol 24:451–468

Paytan A (2000) Sulfate clues for the early history of atmospheric oxygen. Science 288:626–627

Paytan A, Kastner M, Campbell D, Thiemens MH (1998) Sulfur isotopic composition of Cenozoic seawater sulfate. Science 282:1459–1462

Pereira Z, Saez R, Pons JM, Oliveira JT, Moreno C (1996) Edad devónica (Struniense) de las mineralizaciones de Aznalcóllar (Faja Pirítica Ibérica) en base a palinología. Geogaceta 20:1609–1612

Pereira Z, Matos J, Fernnades P, Oliveira JT (2008) Palynostratigraphy and systematic palynology of the Devonian and Carboniferous sucessions of the South Portuguese Zone, Portugal. Memorias do Instituto de Engenharia, Tecnologia e Inovaçao:181

Polag D, Heuwinkel H, Laukenmann S, Greule M, Keppler F (2013) Evidence of anaerobic syntrophic acetate oxidation in biogas batch reactors by analysis of ^{13}C carbon isotopes. Isot Environ Health Stud 49:365–377

Potter R (1977) An electrochemical investigation of the system copper-sulfur. Econ Geol 72:1524–1542

Pracht J, Boenigk J, Isenbeck-Schröter M, Keppler F, Schöler HF (2001) Abiotic Fe(III) induced mineralization of phenolic substances. Chemosphere 44:613–619

Putnis A (2009) Mineral replacement reactions. Rev Mineral Geochem 70: 87–124

Quesada C (1998) A reappraisal of the structure of the Spanish segment of the Iberian Pyrite Belt. Mineral Deposita 33:31–44

Rahmdor P (1980) The ore minerals and their intergrowths. Pergamon Press

Raiswell R, Plant J (1980) The incorporation of trace elements into pyrite during diagenesis of black shales, Yorkshire, England. Econ Geol 75:684–699

Rasmussen B (2000) Filamentous microfossils in a 3,235-million-year-old volcanogenic massive sulphide deposit. Nature 405:676–679

Reed M, Rusk B, Palandri J (2013) The Butte magmatic-hydrothermal system: one fluid yields all alteration and veins. Econ Geol 108: 1379–1396

Reith F, Fairbrother L, Nolze G, Wilhelmi O, Clode PL, Gregg A, Parsons JE, Wakelin SA, Pring A, Hough R, Southam G, Brugger J (2010) Nanoparticle factories: biofilms hold the key to gold dispersion and nugget formation. Geology 38:843–846

Relvas J (1991) Estudo Geológico e Metalogenético da Área de Gavião, Baixo Alentejo Unpublished MSc thesis. University of Lisbon, Portugal, **248 p**

Révész K, Haiping Q (2007) Determination of the $\delta(^{34}S/^{32}S)$ of sulfate in water: RSIL Lab Code 1951. In: Révész K, Koplen TB (eds) Methods of the Reston Stable Isotope Laboratory: Reston, Virginia, USGS Techniques and Methods, book 10, sec C, chap 10. pp 33

Roland GW (1970) Phase relations below 575 degrees C in the system Ag-As-S. Econ Geol 65:241

Rosa CJP, McPhie J, Relvas JMRS (2010) Type of volcanoes hosting the massive sulfide deposits of the Iberian Pyrite Belt. J Volcanol Geotherm Res 194:107–126

Roseboom EH (1966) An investigation of the system Cu-S and some natural copper sulfides between 25 degrees and 700 degrees C. Econ Geol 61:641–672

Roveri M, Lugli S, Manzi V, Gennari R, Schreiber BC (2014) High-resolution strontium isotope stratigraphy of the Messinian deep Mediterranean basins: implications for marginal to central basins correlation. Mar Geol 349:113–125

Rudnicki MD, Elderfield H, Spiro B (2000) Fractionation of sulfur isotopes during bacterial sulfate reduction in deep ocean sediments at elevated temperatures. Geochim Cosmochim Acta 65:777–789

Rye RO, Bethke PM, Wasserman MD (1992) The stable isotope geochemistry of acid sulfate alteration. Econ Geol 87:225–262

Sáenz de Galdeano C, Vera JA (1992) Stratigraphic record and palaeogeographical context of the Neogene basins in the Betic Cordillera. Basin Res 4:21–36

Sáez R, Almodovar GR, Pascual E (1996) Geological constraints on massive sulphide genesis in the Iberian Pyrite Belt. Ore Geol Rev 11:429–451

Salata GG, Roelke LA, Cifuentes LA (2000) A rapid and precise method for measuring stable carbon isotope ratios of dissolved inorganic carbon. Mar Chem 69:153–161

Sánchez España J, Lopez Pamo E, Santofimia E, Diez Ercilla M (2008) The acidic mine pit lakes of the Iberian Pyrite Belt: an approach to their physical limnology and hydrogeochemistry. Appl Geochem 23:1260–1287

Sato M (1960) Oxidation of sulfide orebodies. Econ Geol 55:928–961

Scheiber L, Ayora C, Vazquez-Suñe E, Cendón DI, Soler A, Custodio E, Baquero JC (2015) Recent and old groundwater in the Niebla-Posadas regional aquifer (southern Spain): implications for its management. J Hydrol 523:624–635

Scott KM, Ashley PM, Lawie DC (2001) The geochemistry, mineralogy and maturity of gossans derived from volcanogenic Zn-Pb-Cu deposits of the eastern Lachlan Fold Belt, NSW, Australia. J Geochem Explor 72:169–191

Sheppard SMF (1986) Characterization and isotopic variations in natural waters. Rev Mineral Geochem 16:165–184

Shock EL (2009) Minerals as energy sources for microorganisms. Econ Geol 104:1235–1248

Sillitoe RH (2005) Supergene oxidized and enriched porphyry copper and related deposits. In: Hedenquist JW, Thompson JFH, Goldfarb RJ, Richards JP (eds) Economic geology—one hundredth anniversary volume pp 723-768

Silva JB, Oliveira JT, Ribeiro A (1990) Structural outline of the South Portuguese Zone. In: Dallmeyer RD, Martinez García E (eds) PreMesozoic geology of Iberia. Springer Verlag, Heidelberg, pp 348–362

Simmons SF, Christenson BW (1994) Origins of calcite in a boiling geothermal system. Am J Sci 294:361–400

Sood MK, Wagner RJ, Markazi HD (1986) Stratabound copper deposits in East South-Central Alaska: their characteristics and origin. In: Friedrich G, Genkin A, Naldrett A, Ridge J, Sillitoe R, Vokes F (eds) Geology and metallogeny of copper deposits. Springer, Berlin, pp 422–442

Southam G, Saunders JA (2005) The geomicrobiology of ore deposits. Econ Geol 100:1067–1084

Southam G, Lengke MF, Fairbrother L, Reith F (2009) The biogeochemistry of gold. Elements 5:303–307

Spiro B, Gibson PJ, Shaw HF (1993) Eogenetic siderites in lacustrine oil shales from Queensland. Australia. A stable isotope study. Chem Geol 106:415–427

Spycher NF, Reed MH (1989) Evolution of a Broadlands-type epithermal ore fluid along alternative P-T paths; implications for the transport and deposition of base, precious, and volatile metals. Econ Geol 84:328–359

Sracek O, Gélinas P, Lefebvre R, Nicholson RV (2006) Comparison of methods for the estimation of pyrite oxidation rate in a waste rock pile at Mine Doyon site, Quebec, Canada. J Geochem Explor 91:99–109

Stetter KO (1996) Hyperthermophilic procaryotes. FEMS Microbiol Rev 18:149–158

Strauss H, Schieber J (1990) A sulfur isotope study of pyrite genesis: the Mid-Proterozoic Newland Formation, Belt Supergroup, Montana. Geochim Cosmochim Acta 54:197–204

Taylor R (2011) Gossans and leached cappings—field assessment. Springer, 165 pp

Taylor GF, Sylvester GC (1982) Analysis of a weathered profile on sulfide mineralization at Mugga Mugga, Western Australia. J Geochem Explor 16:105–134

Thieblemont D, Pascual E, Stein G (1998) Magmatism in the Iberian Pyrite Belt: petrological constraints on a metallogenic model. Mineral Deposita 33:98–110

Titley SR, Beane RE (1981) Porphyry copper deposits. Part I: Geologíc settings, petrology and tectogenesis. In: Skinner BJ (ed) Econ Geol 75th Anniversary Volume, pp 214-234

Tornos F (2006) Environment of formation and styles of volcanogenic massive sulfides: the Iberian Pyrite Belt. Ore Geol Rev 28:259–307

Tornos F, Gonzalez Clavijo E, Spiro BF (1998) The Filón Norte orebody (Tharsis, Iberian Pyrite Belt): a proximal low-temperature shale-hosted massive sulphide in a thin-skinned tectonic belt. Mineral Deposita 33:150–169

Tornos F, Solomon M, Conde C, Spiro BF (2008) Formation of the Tharsis massive sulfide deposit, Iberian Pyrite Belt: Geological, lithogeochemical, and stable isotope evidence for deposition in a brine pool. Econ Geol 103:185–214

Tornos F, Miguelez NG, Velasco F, Videira JC (2011) Biogenic supergene galena-rich ore in the Las Cruces deposit, Spain. Min Mag 75:2024

Tornos F, Velasco F, Miguelez NG (2012a) The secondary high-grade Cu deposit of Las Cruces (S Spain): a VMS deposit with superimposed epithermal-like present-day mineralization. Abstracts European Mineralogical Conference, 1: EMC2012-251. Frankfurt

Tornos F, Velasco F, Miguelez NG (2012b) Secondary vs supergene ore enrichment. The high grade Cu ores of Las Cruces mine (S Spain). Abstract SEG Conference Lima

Tornos F, Velasco F, Miguelez NG, Escobar JM (2013) Polyphase secondary alteration and the formation of complex Cu and Pb-Ag-Au-rich assemblages, Las Cruces copper deposit, SW Spain Mineral Deposit Research for a High Tech World -12th SGA Biennial Meeting 2013 pp 587-589

Tornos F, Velasco F, Menor-Salvan C, Delgado A, Slack JF, Escobar JM (2014) Formation of recent Pb-Ag-Au mineralization by potential sub-surface microbial activity. Nat Commun 5:4600. doi:10.1038/ncomms5600

Turpin L, Leroy JL, Sheppard SMF (1990) Isotopic systematics (O, H, C, Sr, Nd) of superimposed barren and U-bearing hydrothermal systems in an Hercynian granite, Massif Central, France. Chem Geol 88:85–98

Valenzuela A, Donaire T, Gonzalez-Roldan MJ, Toscano M, Pascual E (2011a) Volcanic architecture in the Odiel river area and the volcanic environment in the Rio Tinto-Nerva Unit, Iberian Pyrite Belt, Spain. J Volcanol Geotherm Res 202:29–46

Valenzuela A, Donaire T, Pin C, Toscano M, Hamilton MA, Pascual E (2011b) Geochemistry and U-Pb dating of felsic volcanic rocks in the Riotinto-Nerva unit, Iberian Pyrite Belt, Spain: crustal thinning, progressive crustal melting and massive sulphide genesis. J Geol Soc 168:717–731

Velasco F, Sanchez España J, Boyce A, Fallick AE, Saez R, Almodovar GR (1998) A new sulphur isotopic study of some Iberian Pyrite Belt deposits: evidence of a textural control on some sulphur isotope compositions. Mineral Deposita 34:1–18

Velasco F, Herrero JM, Suarez S, Yusta I, Alvaro A, Tornos F (2013) Supergene features and evolution of the gossans capping the massive sulphide deposits of the Iberian Pyrite Belt. Ore Geol Rev 53:181–203

Viñals J, Roca A, Cruells M, Núñez C (1995) Characterization and cyanidation of Rio Tinto gossan ores. Can Metall Q 34:115–122

Williams D (1934) The geology of the Rio Tinto mines, Spain. Trans Inst Min Metall 43:b593–b678

Winter LS, Tosdal RM, Mortensen JK, Franklin JM (2004) Volcanic stratigraphy and geochronology of the Cretaceous Lancones basin, Northwestern Peru: Position and timing of giant VMS Deposits. Econ Geol 105:713–742

Yapp CJ (1987) Oxygen and hydrogen isotope variations among goethites (α-FeOOH) and the determination of paleotemperatures. Geochim Cosmochim Acta 51:355–364

Yapp CJ (2007) Oxygen isotopes in synthetic goethite and a model for the apparent pH dependence of goethite–water $^{18}O/^{16}O$ fractionation. Geochim Cosmochim Acta 71:1115–1129

Yesares L, Nieto JM, Saez R, Almodovar GR, Videira JC (2011a) El Gossan de "Las Cruces" (Faja Piritica Ibérica): Litología y Evolución Mineralógica. Macla 13:225-226

Yesares L, Nieto JM, Saez R, Almodovar GR, Videira JC (2011b) Enriquecimiento de Au-Ag-Hg en el Gossan de Las Cruces (Sevilla). Macla 15

Yesares L, Sáez R, Nieto JM, de Almodóvar GR, Cooper S (2014) Supergene enrichment of precious metals by natural amalgamation in the Las Cruces weathering profile (Iberian Pyrite Belt, SW Spain). Ore Geol Rev 58:14–26

Yesares L, Sáez R, Nieto JM, De Almodovar GR, Gómez C, Escobar JM (2015) The Las Cruces deposit, Iberian Pyrite Belt, Spain. Ore Geol Rev 66:25–46

Zehnder AJB, Brock TD (1980) Anaerobic methane oxidation: occurrence and ecology. Appl Environ Microbiol 39:194–204

Zheng YF (1993) Calculation of oxygen isotope fractionation in anhydrous silicate minerals. Geochim Cosmochim Acta 57: 1079–1091

Zierenberg RA, Schiffman P (1990) Microbial control of silver mineralization at a sea-floor hydrothermal site on the northern Gorda Ridge. Nature 348:155–157